



UNIVERSIDAD DE CHILE
FACULTAD DE CIENCIAS FÍSICAS Y MATEMÁTICAS
DEPARTAMENTO DE INGENIERÍA CIVIL

**STRUCTURAL HEALTH MONITORING OF SOUTH AMERICA'S
FIRST 6-STORY EXPERIMENTAL LIGHT-FRAME TIMBER-
BUILDING BY USING A LOW-COST RASPBERRYSHAKE SEISMIC
INSTRUMENTATION**

TESIS PARA OPTAR AL GRADO DE MAGÍSTER EN CIENCIAS DE LA
INGENIERÍA, MENCIÓN INGENIERÍA ESTRUCTURAL, SÍSMICA Y GEOTÉCNICA
MEMORIA PARA OPTAR AL TÍTULO DE INGENIERO CIVIL

MATÍAS NICOLÁS ALARCÓN DÍAZ

PROFESOR GUÍA:

FRANCISCO HERNÁNDEZ PRADO

PROFESOR CO-GUÍA:

PABLO GUINDOS BRETONES

MIEMBROS DE LA COMISIÓN:

JOSÉ LUIZ ALMAZÁN CAMPILLAY

PEDRO SOTO MUÑOZ

Este trabajo ha sido financiado por el Centro Nacional de Excelencia para la Industria de la Madera (ANID Basal FBA210015) y el Centro UC de Innovación en Madera

SANTIAGO DE CHILE

2022

RESUMEN DE LA TESIS PARA OPTAR AL GRADO DE: MAGÍSTER EN INGENIERÍA ESTRUCTURAL, SÍSMICA Y GEOTÉCNICA
MEMORIA PARA OPTAR AL TÍTULO DE: INGENIERO CIVIL
POR: MATÍAS NICOLÁS ALARCÓN DÍAZ
FECHA: 2022
PROFESOR GUÍA: FRANCISCO HERNÁNDEZ PRADO

MONITOREO DE LA SALUD ESTRUCTURAL DEL PRIMER EDIFICIO DE MADERA EXPERIMENTAL EN SISTEMA MARCO-PLATAFORMA DE 6 PISOS DE AMÉRICA DEL SUR, MEDIANTE EL USO DE INSTRUMENTACIÓN SÍSMICA DE BAJO COSTO

El presente trabajo de título describe la implementación y validación de un sistema de instrumentación sísmica de bajo costo (SISBC) para el monitoreo de la salud estructural del primer edificio experimental de madera de estructura ligera de 6 pisos de América del Sur (Torre Peñuelas). Además, el acoplamiento del SISBC con un sistema de medición de temperatura y humedad relativa ha permitido investigar las variaciones de las propiedades dinámicas del edificio inducidas por el ambiente. El SISBC se ha realizado utilizando seis acelerógrafos RaspberryShake® R4SD (R4SD), que se interconectaron mediante una red local controlada por una Raspberry Pi3 (RPi3) auxiliar. La función del RPi3 consiste en: (i) actuar como un servidor NTP que permite la sincronización de los instrumentos sísmicos; (ii) estar conectado a Internet para proporcionar control remoto y comunicación; (iii) estimar las propiedades dinámicas del edificio utilizando el método FDD a partir de pruebas de vibración ambiental por hora basadas en los datos de velocidad obtenidos de los geófonos verticales incluidos en los instrumentos R4SD. El SISBC se alimenta eléctricamente mediante una batería y un cargador de batería para garantizar la operatividad durante los cortes de energía. Las frecuencias naturales y las formas modales del edificio se identificaron a partir de análisis modales operativos de cinco pruebas de vibración ambiental integradas, medidas por un sistema de instrumentación sísmica convencional (Episensors ES-U2), que muestran propiedades dinámicas consistentes. Además, el SISBC también fue validado contra pruebas de mesa vibratoria, observándose una buena concordancia para frecuencias de señal menores a 25-30 Hz en comparación con los sistemas de medición convencionales, así como midiendo la respuesta durante un sismo de baja intensidad $M_w=4.6$. Una vez que se validó el SISBC, se agregó un sensor BME280 para monitorear continuamente la temperatura y la humedad relativa dentro del edificio, lo que permitió implementar un sistema de monitoreo de salud estructural para rastrear las variaciones inducidas por el ambiente de las tres frecuencias naturales principales. Se determinó una alta sensibilidad de las frecuencias naturales del edificio debido a las variaciones ambientales, exhibiendo variaciones diarias pico a pico de 9.5-10.9% y variaciones promedio de 25.2-29% durante un período de siete meses, evidenciando así que las estructuras de madera podrían ser más susceptibles a las variaciones de temperatura y humedad relativa que otros sistemas estructurales. Inesperadamente, se descubrió que la estructura de madera era más rígida en condiciones de humedad, lo que puede atribuirse al endurecimiento de los ensamblajes de madera debido a la hinchazón de la madera. Se construyó un modelo de espacio-estado de 24 horas para calcular con precisión las frecuencias naturales estimadas en función de la temperatura y la humedad relativa registradas, lo que demuestra que este procedimiento podría usarse para desagregar de manera efectiva las variaciones inducidas por el ambiente de cambios generados por daños u otras fuentes desconocidas.

Palabras clave: *Instrumentación sísmica de bajo costo, RaspberryShake, Monitoreo de salud estructural, Test de vibraciones ambientales, Edificio de madera de entramado ligero, Análisis modal operativo.*

STRUCTURAL HEALTH MONITORING OF SOUTH AMERICA'S FIRST 6-STORY EXPERIMENTAL LIGHT-FRAME TIMBER- BUILDING BY USING A LOW-COST RASPBERRY SHAKE SEISMIC INSTRUMENTATION

Matías Alarcón ^{a,b}, Pedro Soto ^a, Francisco Hernández ^a, Pablo Guindos ^{b,c,d}

^a Department of Civil Engineering, University of Chile, Av. Blanco Encalada 2002, Santiago 8370449, Chile

^b Centro Nacional de Excelencia para la Industria de la Madera (CENAMAD), Av. Vicuña Mackenna, Santiago 7820436, Chile

^c Department of Structural and Geotechnical Engineering, Pontificia Universidad Católica de Chile, Av. Vicuña Mackenna, Santiago 7820436, Chile

^d Department of Construction Engineering and Management, Pontificia Universidad Católica de Chile, Av. Vicuña Mackenna, Santiago 7820436, Chile

Abstract

A low-cost seismic instrumentation system (LCSIS) has been implemented and validated for the structural health monitoring of South America's first experimental 6-story light-frame timber building (Peñuelas Tower). Furthermore, coupling the LCSIS with relative humidity and temperature measuring system has allowed for investigating the ambient-induced variations of the building's dynamic properties. The LCSIS has been accomplished using six accelerographs RaspberryShake® R4SD (R4SD), which were interconnected using a local network controlled by an auxiliary Raspberry Pi3 (RPi3). The function of the RPi3 consisted of: (i) acting as an NTP server that allowed for synchronization of the seismic instruments; (ii) being connected to the internet to provide remote control and communication; (iii) estimating the dynamic properties of the building by using the FDD method from hourly ambient vibration tests based on the velocity data obtained from the vertical geophones included in R4SD instruments. The LCSIS was electrically supplied using a battery and a battery charger to ensure operability during power outages. The building's natural frequencies and mode shapes were identified from operational modal analyses of five integrated ambient vibration tests, measured by a conventional seismic instrumentation system (Episensors ES-U2), showing consistent dynamic properties. Furthermore, the LCSIS was also validated against shake table tests, observing a good agreement for signal frequencies smaller than 25-30 Hz in comparison with conventional measuring systems as well as measuring the response during an earthquake of low-intensity $M_w=4.6$. Once the LCSIS was validated, a BME280 sensor was added to continuously monitor the temperature and relative humidity inside the building, which allowed for the implementation of a structural health monitoring system to track the ambient-induced variations of three principal natural frequencies. It was found a high sensitivity of the building's natural frequencies due to ambient variations, exhibiting peak-to-peak daily variations of 9.5-10.9% and average variations of 25.2-29% during a seven-month period, thus evidencing that timber structures could be more susceptible to temperature and relative humidity variations than other structural systems. Unexpectedly, the timber structure was found to be stiffer under moist conditions, which may be attributed to the tightening of timber assemblies due to wood swelling. A 24-hour state-space model was built to accurately compute the estimated natural frequencies as a function of the recorded temperature and relative humidity, showing that this procedure could be used to effectively disaggregate the ambient-induced variations from changes generated by damage or other unknown sources.

Keywords: *Low-cost seismic Instrumentation, RaspberryShake, Structural Health Monitoring, Ambient Vibration Test, Light-Frame Timber-Building, Operational Modal Analysis.*

“Die Philosophen haben die Welt nur verschieden interpretiert, es kömmt aber darauf an, sie zu verändern”

“Los filósofos no han hecho más que interpretar de diversos modos el mundo, pero de lo que se trata es de transformarlo”

AGRADECIMIENTOS

Los grandes logros nunca son fruto de los esfuerzos de un individuo, son más bien el resultado de la convolución de múltiples voluntades que de forma consciente o inconsciente, aportaron al éxito de una meta o proyecto. Así lo siento en el caso de mi paso por la Universidad y la finalización de este Trabajo de Título. Son tantos los años de estudio, tantas las dificultades superadas y los seres queridos que me ayudaron a superarlas, que no puedo sino dedicarles este escrito y darles las más profundas gracias. Este trabajo les pertenece tanto ustedes como a mí.

Comienzo por agradecer al profesor Francisco Hernández, por su tremenda dedicación a sus estudiantes, su paciencia y ganas de enseñar. Al profesor Pablo Guindos, por enseñarme el mundo de la construcción en madera y darme la oportunidad de desarrollar mi profesión en él. Al profesor Pedro Soto, por su generosidad al compartir sus conocimientos y experticia técnica en el desarrollo de la instrumentación técnica de Peñuelas.

No estaría aquí sin quienes fueron mis compañeros de ruta desde aquellos días de ensayos PSU, viajes a Rancagua y Preumat, pasando por los gloriosos días del 14A y que hasta el día de hoy han sido una fuente de apoyo, charlas filosóficas y risas. Mis queridos amigos de Rengo: Stefano, Isaías, Pablo, Gonzalo, Meli, Nacho, Iván, Ricardo, Leo y Javi. Mis cabros eléctricos, estén donde estén cumpliendo sus metas espero que siempre haya un tiempo para compartir junto a unas chelitas heladas.

Llegar a Santiago a un nuevo entorno donde no conoces a nadie puede significar una dificultad adicional a la ya exigente tarea de estudiar en Beauchef. Por suerte, conocí gente increíble que me facilitó este arduo camino. Doy las gracias a mi amigo Claudio Elicura, a quién conocí en un somnífero laboratorio en el ya lejano primer año de Plan Común y con quién e vivido muchas aventuras y desventuras. Y por supuesto no puedo dejar de mencionar a mi querido Team Πηγα, Angi, Chalo, David, Cony, Lupi, Ale, Kathy, Pipe y César. Hicieron que mi paso por Ingeniería Civil estuviera lleno de alegrías y ganas de aprender, siempre les agradeceré el gran compañerismo a la hora de enfrentar juntos los múltiples proyectos, informes y tareas de esta ardua carrera. P.D: lo de las chelas también va dirigido a ustedes jaja.

Continuo este agradecimiento con mi amada familia. Agradezco a mi Madre, Paula, por su altruista dedicación y amor a nosotros, tus hijos. Gracias mamá por brindarme una vida llena de alegrías y colores. Agradezco a mi Padre, Víctor, por siempre estar presente cuando lo necesito, eres un sabio consejero, amigo y ejemplo. A mi abuela, Olga de las Mercedes, mi primera maestra en la vida, la mujer que inculcó en mí el amor por el conocimiento, creando en mí un poderoso ímpetu por descubrir el mundo desde que tengo uso de razón. A mi abuela Judy, mi querida Lely Yuyi, quién siempre abre su inmenso corazón para alegrar el día a sus nietos, gracias Lely por tanto amor y por tus sobres, que en más de una ocasión me sacaron de un apuro. Agradezco a mi querida tía Jani, cuyo optimismo, carisma y afecto levantan hasta el más pesimista de los ánimos.

Agradezco a mis hermanas, Francisca, Fernanda y Macarena, mis chicas lindas que siempre me sorprenden por su creatividad y calidez. Cuenten siempre con su hermano mayor, quien las adora y siempre estará para echarles una mano.

Finalmente, le agradezco desde lo más profundo de mi corazón a ella, la que en este tiempo ha sido mi amiga, colega, terapeuta, entrenadora, maestra, pareja y tantas cosas más, mi mundo entero, mi sostén y refugio. Katherine, mi querida colorina, sin ti esto no hubiera sido posible.

Table of Content

1	Introduction	1
2	Experimental Peñuelas Tower Description	3
3	Operational Modal Analysis.....	5
4	Low-cost seismic instrumentation system (LCSIS) using R4SD accelerographs	8
5	LCSIS validation and sensitivity	12
6	Structural Health Monitoring Implementation and Results	14
7	Conclusions	19
8	Acknowledgments.....	20
9	Bibliography.....	21

1 Introduction

Targeting taller timber buildings is a relevant trend in the construction industry and scientific community. As reported in recent reviews [1], about two hundred multi-story timber buildings above five stories and up to 24 stories have been constructed worldwide since 2004. The main reason for the reconsideration of timber for higher rises is the development of new stiffer and stronger structural systems such as cross-laminated systems (CLT) and hybrid concrete-timber systems, among others [2], as well as the widely recognized need for reducing the carbon footprint of the construction industry [3]. In addition, timber is often seen as a sustainable construction material because timber construction products typically entail less embodied energy [4,5], and timber assemblies typically provide thermally insulated layers, thus leading to less operational energy expenditures [6]. However, the variation of the dynamic properties may be especially relevant for timber buildings because wood is commonly more affected than other materials by climatic and service conditions due to its organic and hygroscopic nature [5]. Furthermore, the effect of service conditions on the mechanical behavior of wood has been widely recognized in structural design codes such as the National Design Specification of the USA (NDS, [7]) or the Eurocode 5 (EN 1995-1-1, [8]). That is, the mechanical properties of timber are commonly evaluated based on the service temperature, moisture, duration of load, and size of structural components.

Although multiple ambient vibration tests (AVT) and forced vibration tests (FVT) have been performed in light-timber buildings [9–12], the long-term variation of the dynamic properties of mid-rise timber-frame structures caused by ambient conditions has been scarcely investigated. The existing AVT studies have mainly focused on identifying the fundamental properties of existing buildings, concluding that the fundamental period could significantly shift from the values prescribed by the Canadian or American seismic codes. Camelo [10] proposed a formula based on ambient vibration tests to calculate the main natural period for low-rise structures subjected to micro-vibrations. Similarly, Hafeez [11,12] suggested another equation that can be applied to mid-rise buildings. Likewise, Ellis and Bougard [9] evaluated the dynamic properties of a timber-frame structure at different stages of construction, concluding that brickwork can increase 17.7 times the stiffness of the building compared to the bare building. However, in structures other than timber, the ambient-induced variations of the dynamic properties have much more comprehensively been investigated, such as RC buildings [13–16], historical structures [17,18], or bridges [19–21]. Overall, RC buildings, historical structures, and bridges have experienced a peak-to-peak daily variation of their natural frequencies of 7%, 8%, and 10%, respectively.

Regarding the FVT in timber buildings, several shake table tests have been accomplished, mainly comprising structures ranging from one-story residential houses to six-story multi-family buildings [22–25]. Apart from determining the seismic structural performance, those investigations have mainly focused on determining the influence of the nonstructural components on the dynamic properties of the timber buildings - which has been found to be a strong influence - without consideration of moisture or temperature variations. Kharrazi [22] and Filiatrault et al. [23] confirmed that the nonstructural components and finishes could drastically modify the initial dynamic properties of timber structures because their stiffnesses are comparable to the stiffness provided by the structural system. Similarly, Christovasilis [24] observed that the peak roof displacement was reduced by 44% when adding gypsum wallboard to the shear wall of a seismically tested two-story house. Likewise, during seismic tests, a fast stiffness degradation is commonly observed because of the fragile response of nonstructural components (e.g., gypsum wallboard and stucco) [22,23]. Overall, timber building damping ratios estimated from seismic tests were remarkably high (10%-20%) [24]. Van de Lindt et al. [25] proposed and validated a Performance-Based Seismic Design procedure for a 6-story NEESWood light-frame timber tested on Japan's E-Defense shake table.

In conclusion, previous research has proposed new analytical equations to estimate the dynamic properties of timber buildings and has investigated the seismic performance of timber buildings with and without the influence of nonstructural components; meanwhile, it remains considerable uncertainty regarding the effect of ambient-induced variations on the dynamic properties for this type of structures. This research gap becomes especially relevant due to the current interest in targeting taller timber buildings. Therefore, further implementation of health monitoring systems is needed for timber structures. The US Geological Survey stated, "Strong-motion recordings of damaging earthquakes in densely urbanized areas are critical for designing earthquake-resistant structures to reduce property loss and casualties from future earthquakes" [26]. Thus, seismic instrumentation should be prioritized in most countries prone to high seismic hazards. Even though Chile is one of the most seismic-prone areas globally (i.e., 7.6 earthquakes $M_w \geq 7.0$ average per decade since 1900), there is a reduced number of structures currently instrumented in Chile. It is mainly explained by the high cost of these projects, a common problem for developing countries. Studying the structural systems and seismic characteristics of ground motions observed in Chile can be significantly different from other seismic regions.

In this context, this research has been focused on the implementation and validation of a low-cost seismic instrumentation system (LCSIS), comprising a system of RaspberryShake R4SD accelerographs (RS4D) controlled by an auxiliary Raspberry Pi3 (RPi3), which are in coupling with a moisture-temperature measuring system. This LCSIS has allowed the structural health monitoring of South America's first 6-story experimental light-frame timber building, the Peñuelas Tower, considering ambient-induced variations of its dynamic properties. Although research has shown that Raspberry Shake instruments have offered a reasonable option for other seismological applications [27,28], there are no available details about implementing buildings using R4SD accelerographs. Therefore, this investigation, apart from the results obtained for the implementation of the timber building itself, provides detailed information regarding the installation and operation process of the low-cost system and its validation against measurements from conventional seismic measuring systems. In addition, detailed information is provided regarding how to ensure synchronization between different instruments, how to provide an efficient power supply during an electric outage, how to provide remote communication and control of equipment, and how to include other types of sensors (to measure temperature and relative humidity) that work in parallel with R4SD accelerographs.

Moreover, an automatic processing tool was encoded to record strong seismic motions and estimate dynamic properties from periodic ambient vibration tests, effectively allowing the implementation of a structural health monitoring system. The sensibility of R4SD accelerographs was verified in a shake table. Furthermore, two QDR equipment were installed besides R4SD accelerographs, proving that the low-cost instrumentation can accurately record intermediate and high-intensity seismic events. Additionally, ambient vibration tests (Section 3) were carried out to estimate the dynamic properties of the Peñuelas Tower that are compared with results obtained from the SHM system (Section 6). The estimated mode shapes experienced a significant vertical motion due to the high slenderness of the building (allowing those vertical geophones incorporated in the R4SD accelerographs to be effectively employed to monitor the natural frequencies of the building from ambient vibration tests). Finally, a space-state model was implemented to estimate the structure's natural frequency variations due to changes in its internal temperature and relative humidity. This tool could be potentially used to disaggregate changes due to environmental effects and potential damage to the structure due to an earthquake or other unknown source.

2 Experimental Peñuelas Tower Description

The Peñuelas Tower is recognized as the first 6-story light-frame building constructed in South America [29]. This timber building is regarded as a pioneering building in the region not only in terms of its height of 19.4 m but also because it has been manufactured and assembled in a highly prefabricated modular construction process (i.e., the construction lasts just one week to erect the main structure). A further particularity is that the Peñuelas Tower is not a residential building but a slender experimental tower that has been employed to study its hydrothermal and acoustic insulation performance, which has been steadily monitored since its construction at the end of 2018. The tower was designed by the Timber Innovation Center UC CIM-UC at the Pontificia Universidad Católica de Chile, and constructed by Tecno Fast S.A., in Santiago, Chile. It represents an iconic national research effort toward fostering the utilization of timber and prefabrication methods in multi-story residential construction. The Tower was built with an assembly of 10 highly industrialized 3D modules, casting a floorplan of 4.96 x 4.96 m. In addition, a sub-structure was installed on the roof made up of timber beams and columns to support an array of solar panels, see Figure 1.

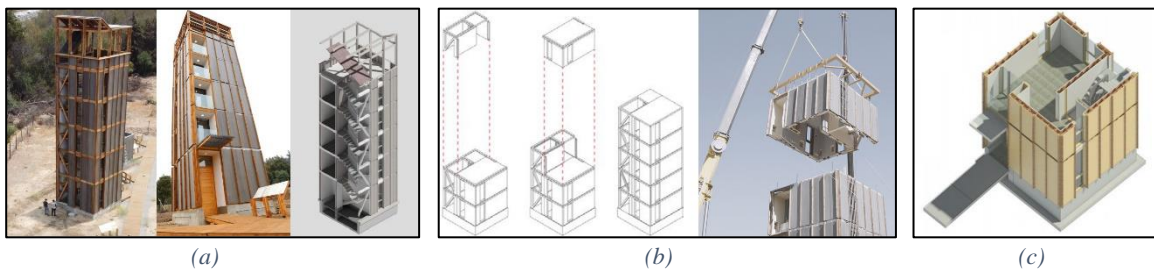


Figure 1: Peñuelas' Tower: (a) Global view of the Tower; (b) Modules assembly process; (c) Section of the Tower

All panel assemblies of the building (slabs, walls, and roof) were made of dimensional lumber (2" or 3" in thickness) of structural Chilean radiata pine mechanically graded as MPG10 according to the Australian standard [30] and C16 according to the European standard [31]. According to the American Plywood Association's certification, sheathing elements consisted of OSB and plywood boards manufactured in Chile and certified as sheathing grade (standards PS1-19 and PS2-18 [32,33]). The typical thickness of the sheathing was 11.1 mm. The nailing of the light frame and sheathing consisted of Nails of 3 x 70 mm, spaced at 50, 100 mm, or 150 mm. Perimetral wall panels were covered at the inner side with double gypsum boards and a thickness of 15 mm for fire protection. Drywall screws type coarse thread #6 x 3" were used for fixing the gypsum board to the wall elements. Roof and slab panels were sheathed with a similar gypsum board configuration only at the bottom side. In order to prevent overturning, the ATS anchorage proprietary system of Simpson Strong-Tie, Pleasanton, CA, United States, was utilized. This anchorage system consists of 1/2" to 1 3/4" diameter steel rods of quality A105. A ventilated façade is installed in the Tower composed of timber elements of various dimensions of thermo-treated radiata pine Termowood® CMPC and Tricoya® MDF panels with acetylated treatment and Leaf Panel stained; the timber elements are arranged in a way that an air gap is created between the MDF panels and the exterior walls of the Tower, creating an effective barrier against the weather. The timber production of the walls and floor panels was manufactured at robotic production lines consisting of a semi-automatic frame assembly and fully automated CNC bridges for nailing the sheathing at the Tecno Fast S.A. production plant in Santiago, Chile. After the wall, slabs, and roof panels were manufactured, they were connected together at the fabrication plant, constituting 3D modules. However, to prevent wall and slab duplication when assembling on-site adjacent 3D modules, the modules lacked one wall and wall slab panel each, see Figure 2. A conventional crane was employed to erect and mount each story over the previous ones. Nonstructural components such as the electrical system and claddings were performed on the field. A summary scheme of the modular construction process is shown in Figure 2.

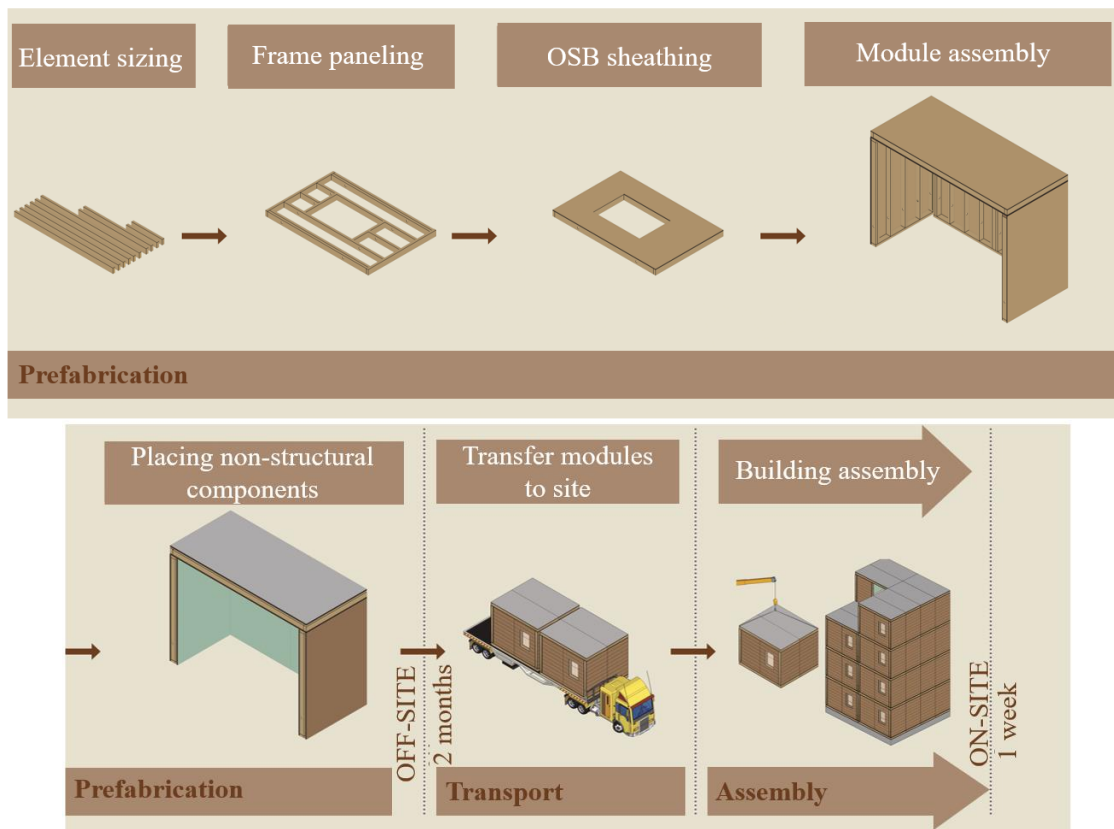


Figure 2: Scheme of the manufacture and construction of the Peñuelas Tower building

Because of the high Chilean seismicity, strong shear walls were used as the primary lateral force resisting system. The strong shear walls were achieved by featuring 38 x 135 mm (2" x 6") and 41 x 185mm (2" x 8") studs as frame members, OSB sheathing at both sides, narrow nailing patterns, and strong rods as tie-down anchoring system, all the details of the walls can be found in [34]. The mechanical properties of this system were extensively tested and can also be found in the literature [35–37]. To provide fire protection, the walls were further covered by two gypsum boards of 15 mm in thickness on the interior side. Drywall screws type coarse thread #6 x 3" were used as connectors between gypsum boards and the timber frame. Apart from the shear walls, some modules of the Tower also included a diagonal timber bracing system comprising beams, columns, and diagonals of 145 to 230 cm² in cross-section, graded as MGP10 according to the Australian standard [30], connected with bolts of 5/8 inches in diameter. Due to the small wall length available, this additional bracing system was necessary to add lateral stiffness to the modules featuring the staircase.

Several slab configurations were used for each floor to test different flooring systems. More specifically, a timber frame with a dimensional 41 x 185 mm cross-section with the same wood material of the shear walls was used for the flooring, but different nonstructural finishes were equipped on each floor to study their thermal transmittance capabilities. As a result, the finishing of the ground floor to the 4th floor was, respectively, ceramic tiles over the concrete floor slab, 41 mm thick fiber cement plates, 41 mm thick prefabricated concrete plates, 15 mm thick plywood panels, ceramic tiles on a layer of 41 mm thick prefabricated concrete plates. Finally, the terrace was equipped with a timber platform on a bed of compact sand with a slope of 2%. Thus, although the same flooring structural system remains in height, the finishing made up an uneven mass distribution, which affects its dynamic behavior. Furthermore, besides the gypsum boards and finishings, other nonstructural components such as moisture barriers and acoustic insulation were added to walls and slabs, adding more nonstructural mass. The full details of the panel configurations can be found in [29,38].

3 Operational Modal Analysis

Five ambient vibration tests were performed in the Peñuelas Tower; see a schematic of each test in Figure 3. The ambient vibration tests were accomplished using 11 or 12 highly sensitive conventional accelerometers Episensor ES-U2 from Kinemetrics [39] (set to a threshold peak acceleration of 0.5g), a Daqbook/2000 acquisition system (16 bits-200kHz, and 16 terminals), and an external laptop with the DaqView software package. For each test, the natural vibration of the structure caused by traffic, micro-tremors, and wind was recorded for 30 minutes at a sampling frequency of 200 Hz. During each ambient vibration test, three referential sensors were kept in the same position (sensors 1,2,3 in Figure 3) and placed on two corners on the fourth floor (to describe longitudinal, transverse, and torsional responses). During each test, the other eight or nine sensors were distributed to different places of the structure. In addition, the vertical motion and bending rotations of each floor were also measured during these tests, considering that the Peñuelas Tower could be significantly susceptible to bending effects because of its slenderness. Moreover, the vertical measurements could be used to validate if the permanent seismic instrumentation (see Section 5) can be potentially used to carry out periodic ambient vibration tests to generate a Structural Health Monitoring (SHM) system. In other words, an SHM system can be built based on the ambient vibration signals recorded from the vertical geophones incorporated in the RaspberryShake R4SD accelerographs (see Section 6). Noting that the MEMS accelerometers incorporated in the R4SD accelerographs display a low Signal-to-Noise ratio, making them unable to be used for ambient vibration purposes. Therefore, verifying if the principal structural modes could be detected by analyzing the vertical movements is pertinent.

The reduced number of available sensors prompted five ambient vibrations tests to estimate the full six-DOF mode shapes of the Tower. First, the horizontal translation movements and torsional rotation were assessed using three horizontal accelerometers installed in two different corners of the measured flooring, see Figure 3. Similarly, three vertical accelerometers were installed in three different corners of the slab when vertical movement and bending rotations were measured, as shown in Figure 3.

The dynamic properties of the Peñuelas Tower (natural frequencies and mode shapes) were estimated by using the Subspace System Identification (SSI) method [40] and the Frequency Domain Decomposition method [41]. Figure 4a shows the stabilization diagram obtained from the SSI method at the left-hand pane. Similitude criteria of 5% for frequency, 5% for damping ratios, and 10% for Modal Assurance Criterion (MAC, Allemang & Brown [42]) are considered to build the Stabilization Diagram assuming a model order between 2 to 240. Figure 4b shows the semi-log plot of the singular values obtained from the FFD method. Figure 4c shows the MAC values to compare the first six mode shapes estimated from SSI and FDD. Both system identification techniques show similar results, validating that an accurate estimation of the dynamic properties has been obtained.

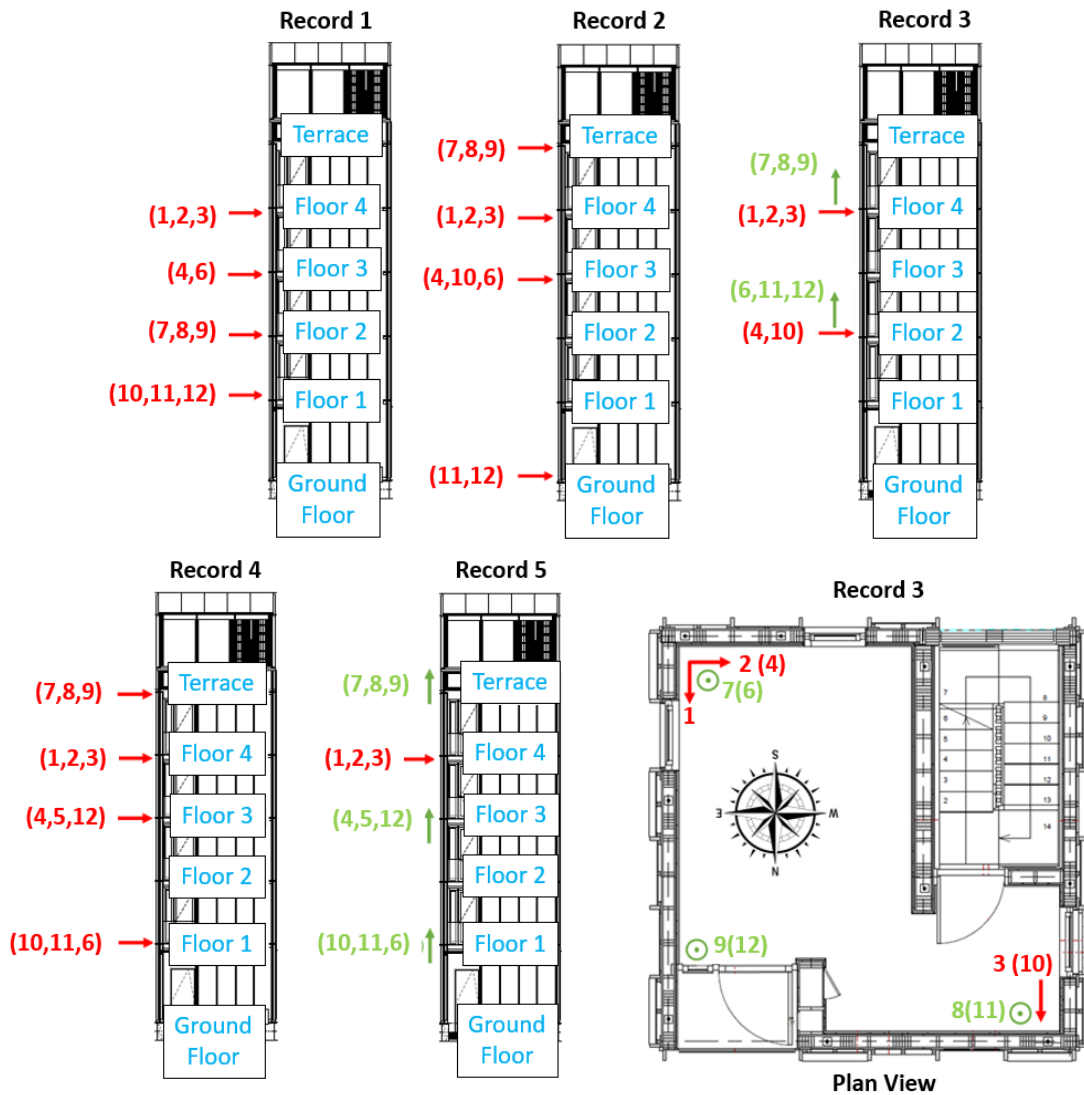


Figure 3: Seismic sensor layout for each ambient vibration test

The ambient vibration tests were performed on two different days. Record 1, Record 2, and Record 3 (Figure 3) were carried out on October 22, 2020 – a relatively cold day with temperatures ranging between 11.7°C and 13.2 °C -, and Record 4 and Record 5 were performed on November 26, 2020, a warm day (27.6-28.4 °C). Table 1 summarizes the range of the nine principal natural frequencies estimated from ambient vibration tests performed on different days. The main estimated natural frequencies were similar to the suggested by the UBCC code (2.651 Hz) [43], and significantly lower than the simplified equations proposed by Camelo (3.693 Hz) [10] and Hafeez (4.719 Hz E-W and 5.985 Hz N-S) [11]. It indicates that the suggested simplified equations could be not applicable for slender light-frame buildings with strong walls. It was also observed that mode shapes were consistent between different measurements and days. Table 1 shows a plan view of the floor movement related to each mode shape and the temperature recorded by a meteorological station (30007) 14km from the Tower during the testing days. A slight variation of frequencies was observed for estimations associated with the same day of testing (which can be related to numerical errors and natural deviations generated by changes in the environmental conditions). However, a significant variation of natural frequencies was observed between different testing days. The average values of the natural frequencies were reduced between 3-9% when the estimations related to the hottest day were compared to the first day of testing. The natural frequencies estimated for the three principal modes

were in the range of variation observed for the SHM system implemented in Section 6 (Figure 13 and Figure 14).

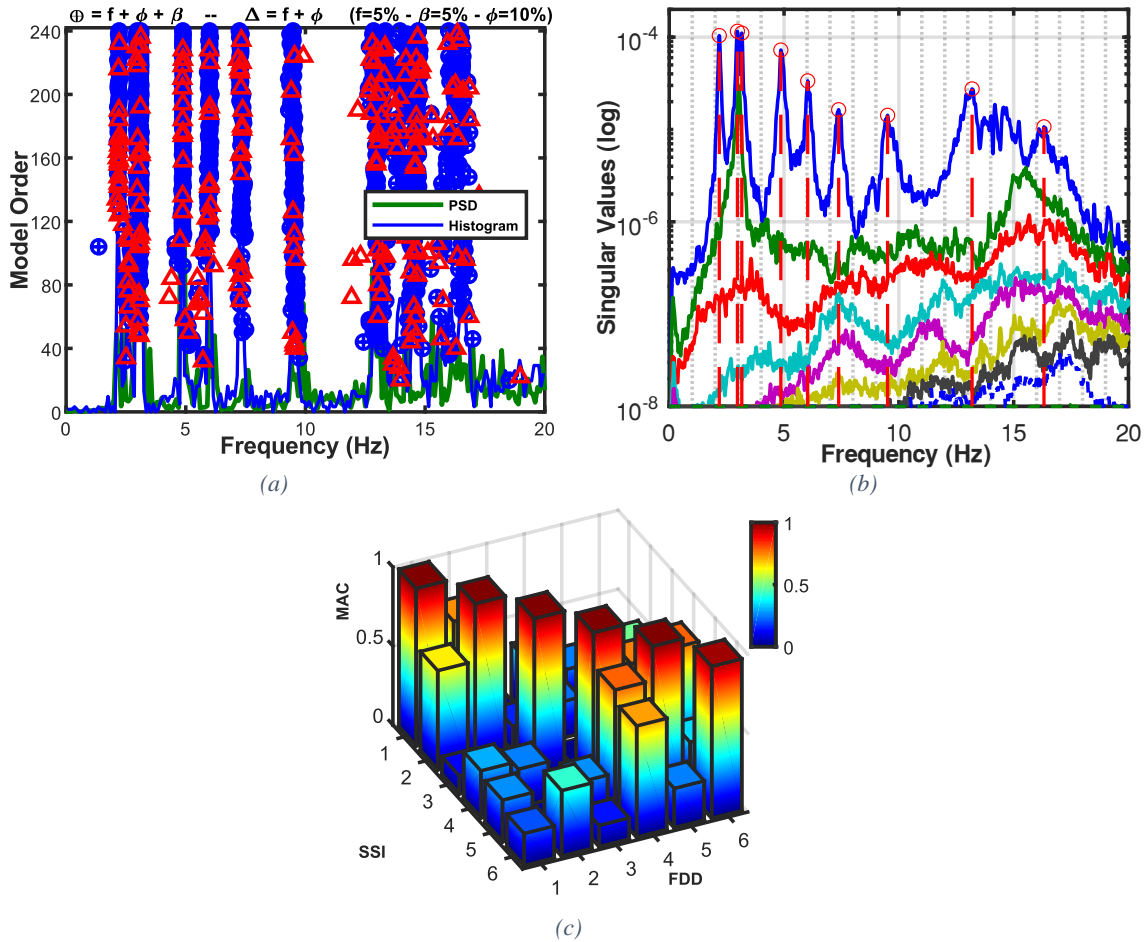
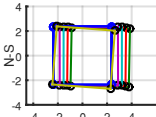
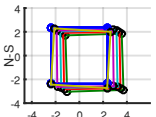
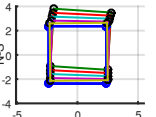
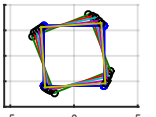
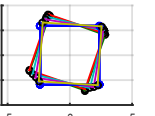
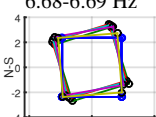
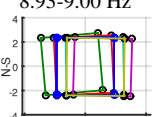
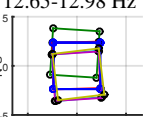
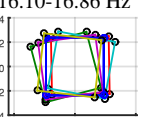


Figure 4: (a) Stabilization Diagram from SSI method; (b) Singular Values from FDD method; (c) MAC comparison between SSI and FDD mode shapes, Record 1

Table 1: Comparison of the frequencies measured during a cold day, dated 22-10-2020 with a daily temperature range of 11.7-13.2 °C, and a warm day, 26-11-2020 with a temperature of 27.6-28.4 °C. Both days showed consistent mode shapes.

Measuring day	Mode 1	Mode 2	Mode 3	Mode 4	Mode 5
Cold day	2.16-2.19 Hz	2.93-2.97 Hz	3.13-3.16 Hz	4.77-4.86 Hz	6.03-6.06 Hz
Warm day	2.02-2.04 Hz	2.81-2.81 Hz	3.01-3.03 Hz	4.56-4.59 Hz	5.63-5.74 Hz
					
	Mode 6	Mode 7	Mode 8	Mode 9	
Cold day	7.18-7.38 Hz	9.38-9.53 Hz	13.19-13.22 Hz	15.63-16.32 Hz	
Warm day	6.68-6.69 Hz	8.93-9.00 Hz	12.65-12.98 Hz	16.10-16.86 Hz	
					

The representation of the 6-DOFs mode shapes obtained for all the Tower floors was built by joining the estimations made from each ambient vibration test. It was successfully implemented by scaling

the mode shape computed for each ambient vibration test to fit the movement associated with the reference floor (longitudinal, transverse, and torsional movements). In other words, the mode shapes were scaled to minimize the difference between the four corner movements computed for the fourth floor. Figure 5a and Figure 5b show a 3D view and a lateral E-W view of the mode shapes. It can be observed that all mode shapes involve the vertical response of the structure to some degree. Thus, it can be concluded that vertical geophones incorporated in the RaspberryShake R4SD instruments could be employed to track the evolution of the dynamic properties, allowing the implementation of the SHM system detailed in Section 6. Similarly, it was observed that the vertical movements experienced by the mode shapes are related to bending effects (which are consistent with the horizontal and torsional movements) due to the high slenderness of the Tower.

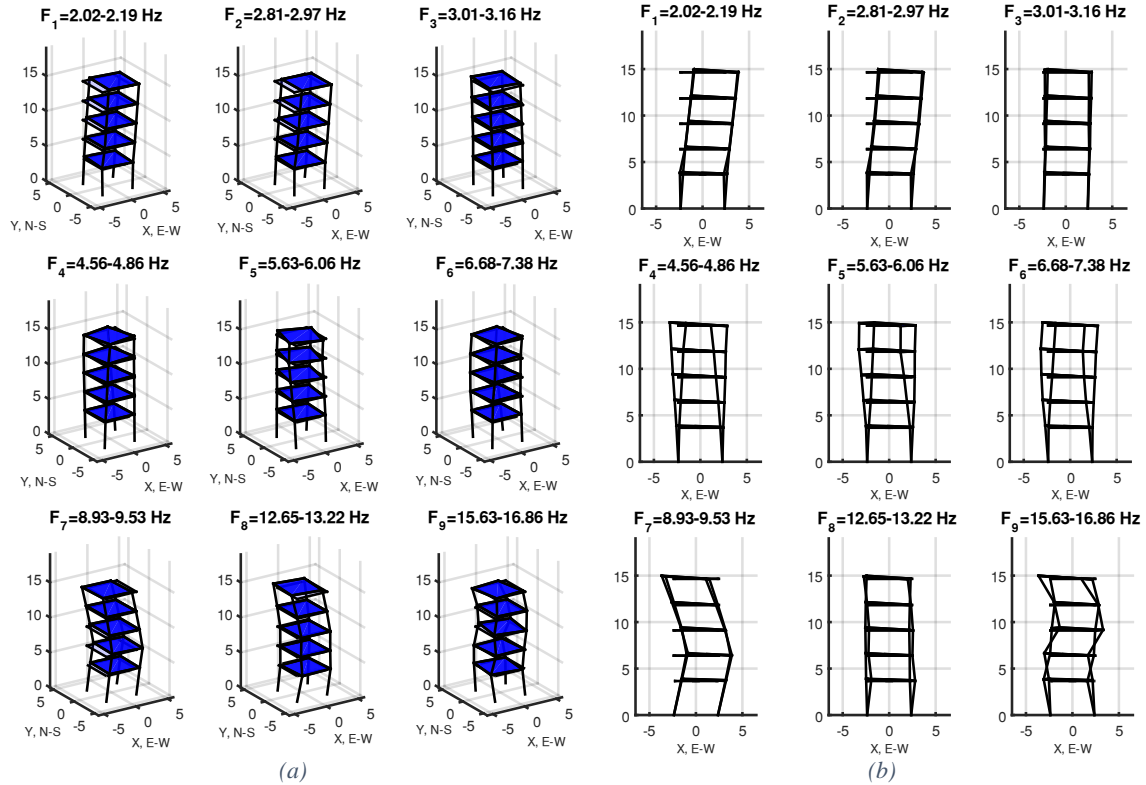


Figure 5: (a) 3D view of mode shapes estimated from AV tests; (b) Lateral view of mode shapes estimated from AV test

4 Low-cost seismic instrumentation system (LCSIS) using R4SD accelerographs

The seismic instrumentation of the Peñuelas Tower was achieved with an LCSIS consisting of Raspberry Shake® RS4D-V8 (RS4D, dynamic range 144 dB-24 bits, DC to 44 Hz) accelerographs [44] made in Panama. The total budget allocated to the seismic instrumentation was approximately USD6000 (for six accelerographs and other complementary equipment described in Figure 6). The R4SD is a promising seismometer and accelerometer with one vertical geophone, a triaxial MEMS accelerometer orthogonally oriented, an acquisition system, and a computer, all in one box. The R4SD accelerographs acquire data to 100 samples per second [45]. The R4SD instruments are accompanied by a Raspberry Pi 3 Model B portable computer (RPi3) that acquires the sensor data and allows communications using the internet or a local network. The disadvantages of MEMS accelerometers are that they do not allow performing ambient vibration tests because of their low signal-to-noise ratio. However, the incorporated vertical geophones allow for estimating natural frequencies from ambient vibration data, as presented in Section 6. The seismic instrumentation was performed using six R4SD, five of them inside the structure (indoor model, Figure 6e, Figure 7d, and Figure 7f) and

another outdoor model (with custom-built IP67 protection, Figure 6j) in a concrete shaft beside the Tower to record the seismic ground motion (Figure 7c). Figure 6 shows the main components used for the seismic instrumentation. Figure 7 shows details about the equipment installation.

The seismic instrumentation was designed to work even if a power outage occurred, which was achieved by using a 12V 55Ah deep cycle battery KBL12260W (Figure 6b and Figure 7a) that supplies energy to the entire seismic instrumentation system. The battery was continuously charged by a battery charger BC25-B2C that is directly connected to the Tower's power supply (Figure 6a and Figure 7a). That is, the R4SD (Figure 6e and Figure 6j), the RPi3 (Figure 7b), the router, and the switch (Figure 6i) are supplied electrically from the battery that works as a UPS (uninterruptible power supply) for the entire system. In this way, the system could operate autonomously for three days without a power supply. Multicore cables TRIMERX CAT6 UTP (Figure 6d and Figure 7d) were employed, using PoE (Power over Ethernet) functionality that safely passes electric power and data to each instrument in one cable. Therefore, PoE injector and splitter devices (Figure 6c, Figure 7d, and Figure 7f) were employed at each cable end to split the Ethernet communication and the electric energy supply (12 V from the battery). The communication path was connected to the R4SD at one end, while the other was plugged to a Router Dlink DIR515 N or the Switch To-link TL-SF1008D (Figure 6i) to create a local network. One end of the electric power path was directly connected to the battery (using a power strip), and the other one was connected to a custom voltage transformer that reduced the supplied voltage from 12 V to 5 V (i.e., the voltage required for the R4SD accelerographs; Figure 7 c, d, and f). A micro-USB cable (Figure 7 d) got from the custom voltage transformer to supply electric energy to the R4SD. Similarly, the RPi3 (Figure 7b) was connected to the router and electrically supplied using the same scheme. The router and switch were likewise connected to custom voltage transformers that were consequently connected to the battery (that reduces the supplied voltage from 12 V to 9 V and 5 V, respectively).

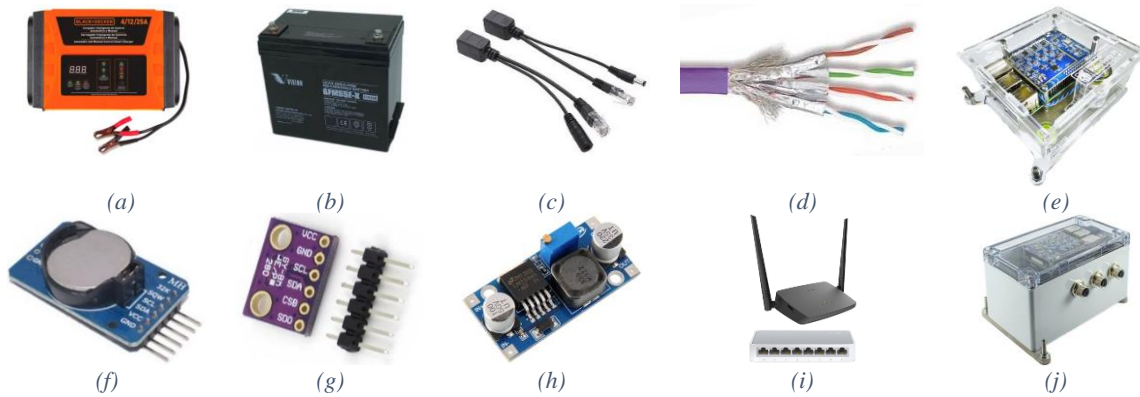


Figure 6: Components of the instrumentation network; (a) BC25-B2C Battery charger; (b) KBL12260W 12v 55Ah deep cycle Battery; (c) PoE Injector/Splitter; (d) TRIMERX UTP cable CAT6; (e) RS4D-V8 instrument with indoor enclosure model; (f) DS3231 precision clock; (g) BME280 sensor; (h) LM2596S 3A step-down module; (i) Router Dlink DIR515N and Switch To-link TL-SF1008D ; (j) RS4D-V8 instrument with outdoor custom-built IP67 enclosure model

A general schematic of distributions of electrical energy, data, and internet networks, related to the seismic instrumentation of the Peñuelas Tower is presented in Figure 8. Figure 9 shows an electrical schematic of the custom voltage transformer (Figure 7e). This latter was based on an adjustable step-down module model LM2596S 3A (Figure 6h and Figure 7e) that could transform an input voltage between 4 and 35 volts into an adjustable output voltage between 1.25 and 30 volts. For security reasons, a fuse holder (Figure 7e) was attached to this module, avoiding electric damage to the R4SD if a sudden amperage increase occurs due to an electric failure.

All instruments were connected to a router or a switch to generate a local internet network (Figure 6i). Then, the RPi3 (Figure 7b) was employed as an NTP server to provide a synchronized time for

all the R4SD. The RPi3 has a mobile broadband modem that allows internet connection, enabling remote equipment control using the Anydesk® software package. R4SD accelerographs were configured to take time from the RPi3 (modifying its hosts' file), ensuring that all sensors share a common time. Therefore, the RPi3 was configured as an NTP server (modifying its ntp.conf). Besides, the RPi3 was also configured to get UTC time from the local SHOA NTP server (ntp.shoa.cl) when the internet was available. If the internet was not available, the RPi3 took the time read from a precision clock model DS3231 (Figure 6f and Figure 7b) that was added to the RPi3. The DS3231 clock has an internal battery; therefore, its time is not lost even if a long-term energy outage occurs, providing the system autonomy even if there was no internet or electric energy for a long-time. It should be taken into account that Raspberry Pi minicomputers do not have a local clock that allows continuous time when turned off, i.e., they continue with the time read before shutting down. Therefore, it is necessary to reestablish their current time using the added DS3231 clock.

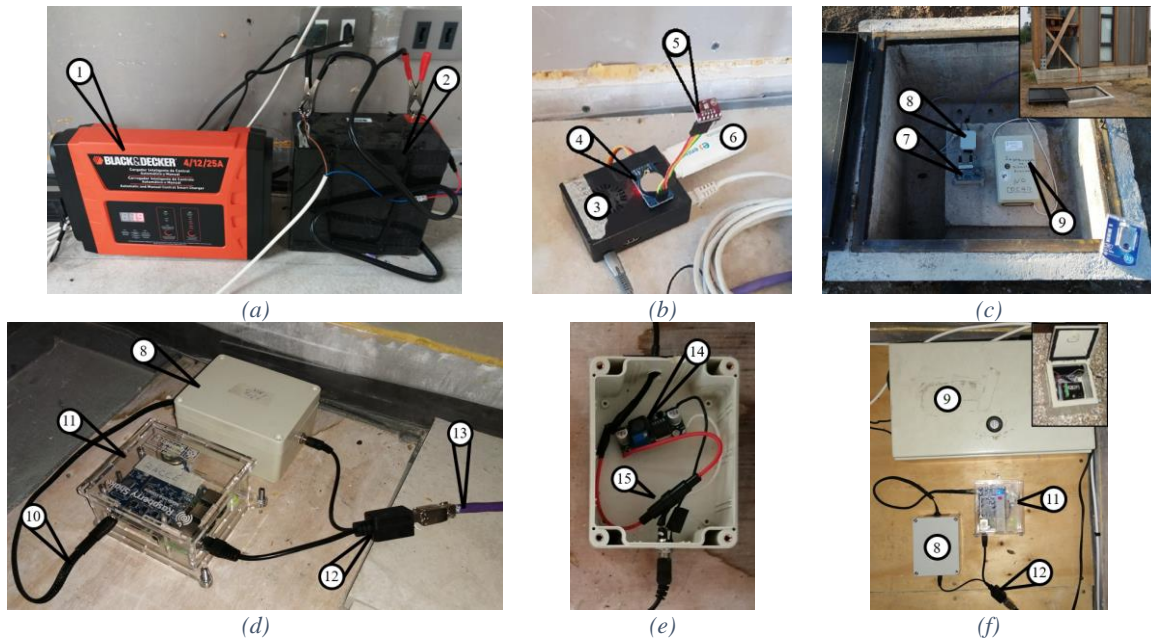


Figure 7: Photographs of Equipment Installation; (1) BC25-B2C battery charger; (2) KBL12260W 12v 55Ah deep cycle battery; (3) Auxiliary Raspberry Pi 3 (4) DS3231 precision clock; (5) BME280 sensor; (6) Mobile broadband modem (7) RS4D-V8 outdoor model accelerograph; (8) Custom voltage transformer (9) QDR accelerograph; (10) Micro-USB; (11) RS4D-V8 indoor model accelerograph; (12) PoE splitter; (13) TRIMERX UTP cable CAT6; (14) LM2596S 3A step-down module; (15) Fuse holder

Another advantage of adding the RPi3 minicomputer connected to a local network (which in turn is connected to the internet providing its remote control using Anydesk [46]) is that it can be used to control all the R4SD remotely. Therefore, the RPi3 allows for checking the synchronization of R4SD equipment (using PuTTY [47]), taking data from equipment (using FTP connection with Filezilla [48] or ObsPy [49]), visualizing real-time data (using Helicorder plot, a web-based application native to the Raspberry Shake instruments and Swarm 3.2.0 [50] software that can be used with Raspberry Shake instruments), and modifying equipment configurations using PuTTY. Finally, a BME280 barometer module (Figure 6g) could be connected to the RPi3 (Figure 7b), allowing real-time barometric pressure, relative humidity, and temperature recording. In this case, the BME280 sensor was placed beside the RPi3, i.e., inside the Tower in the second story. Thus, these measurements (relative humidity and temperature inside the building) could be used to study the evolution of natural frequencies with the variation of environmental conditions (see section 6), enabling for a Structural Health Monitoring system. It should be pointed out that the versatility offered by the Raspberry Pi minicomputers allows for including multiple sensors (strain gauges, LVDT, accelerometers, force

transducer, etc.) that can be combined with the seismic instrumentation (with RaspberryShake instruments). i.e., other Raspberry Pi minicomputers with additional sensors can be included in the local network in order to monitor other variables of interest.

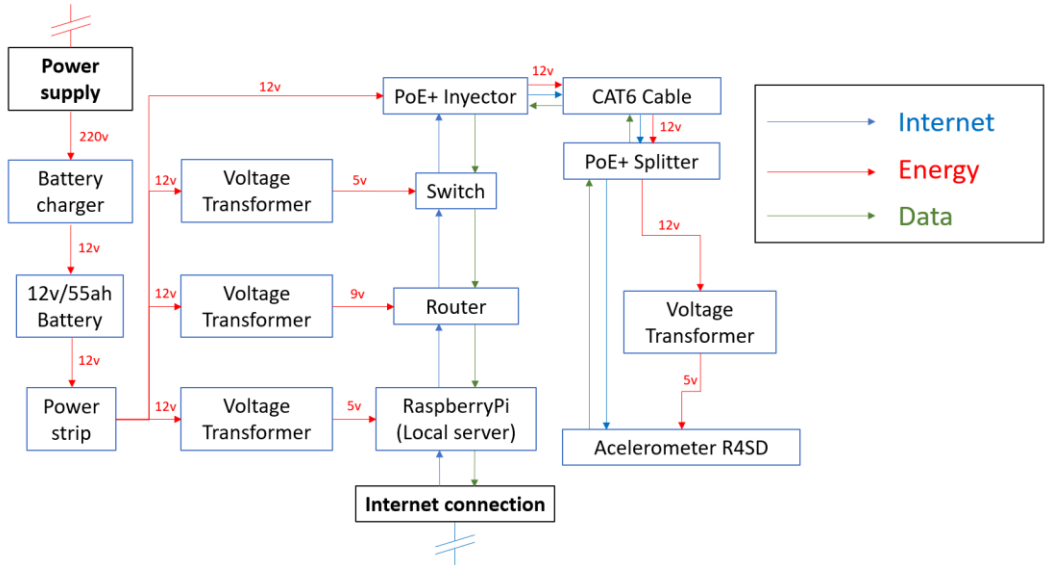
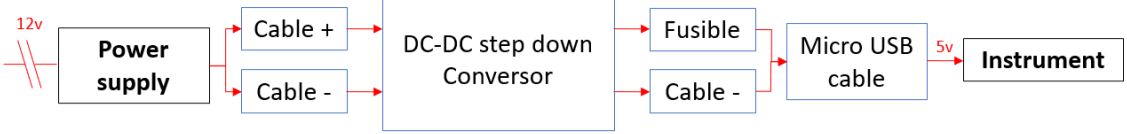


Figure 8: Instrumentation network design scheme



(b)
Figure 9: Custom voltage transformer scheme

Furthermore, the RPi3 can be encoded to perform multiple periodic processes (using crontab). Thus, the RPi3 was encoded using Python [51] and ObsPy, which checked every 5 minutes if the horizontal acceleration traces related to the ground floor R4SD accelerograph had reached a value higher than a predefined threshold (0.005g). If that is the case, the seismic data for all sensors are automatically saved in a designated folder inside the RPi3, and a warning email is automatically sent to advise about the occurrence of a seismic event. Second, ambient vibration (AV) data 30-minutes long was extracted every hour (using Python and ObsPy) related to the incorporated geophones for all active R4SD. This AV data was then processed in the RPi3 to perform the SHM system described in section 6.

Two QDR [52] accelerographs (from Kinometrics®) were installed: one beside the ground floor R4SD accelerograph and another beside one of the R4SD instruments placed on the fourth floor (Figure 10). Therefore, QDR instruments were used to validate the field's LCSIS provided by the R4SD accelerographs (section 5). The local Chilean net of accelerographs (RENADIC) has employed these QDR accelerographs since the 90's decade. They have been effectively used to record multiple seismic events. However, the QDR accelerograph has a few limitations because of its age, including a low signal-to-noise ratio, limited bandpass filter of 1-15 Hz [52], and low resolution for small intensity seismic events (11 bits, 60dB, $f_n=25.4$ Hz, Bandwidth 25 Hz).

The location of the accelerographs (Figure 10) was chosen based on the need to study the seismic response of the Peñuelas Tower. In particular, the local response of the anchor tie-down (ATS) devices from the Simpson Strong-tie® company were the primary concern due to their relevant role in preventing the Tower's overturning (rocking). For this reason, three instruments were installed on the first floor (second story) to measure its bending rotations and vertical response. Moreover, they

allowed analyzing the first story's nonlinear response from the relative response related to the ground floor. In addition, two accelerographs were placed on the third floor to measure the global response of the building. It should be taken into account that the third floor displays significant seismic participation according to the mode shapes estimated from the AV tests described in section 3. Thus, they could be used to capture the structural mode responses described in Figure 5. Similarly, the incorporated geophones could be used to track the principal modal responses from ambient vibration records (section 6). Note that due to logistical constraints, these sensors were installed on the third floor rather than any other upper floor.

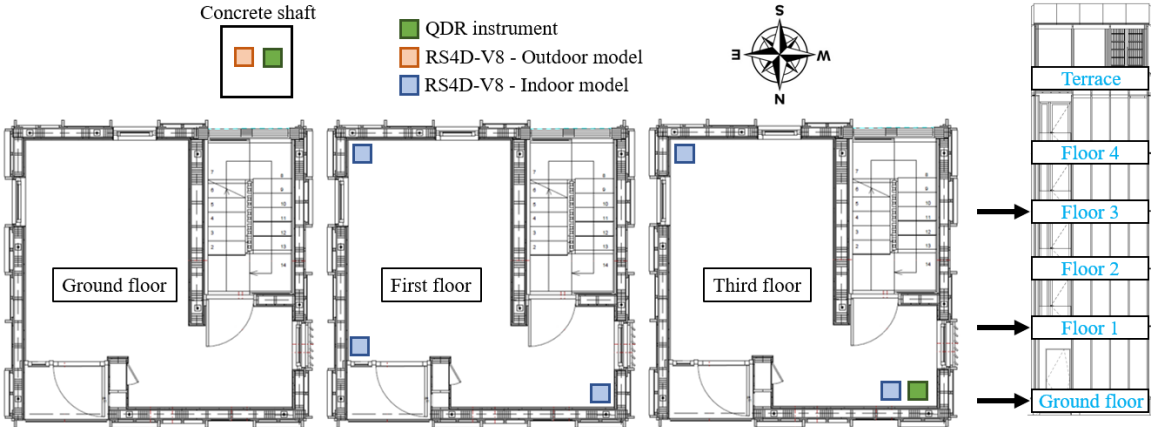


Figure 10: Location of the seismic instruments installed in Peñuelas Tower

5 LCSIS validation and sensitivity

Before accomplishing the Tower's instrumentation, the LCSIS was tested in the laboratory to determine its sensitivity to measuring seismic events. Therefore, multiple shake table tests were performed in which the R4SD were compared with high-quality Episensor ES-U2 accelerometers from Kinematics (the same used for the campaign of ambient vibration tests, in section 3). The shake table tests were performed in the Civil Engineering Department of the University of Chile in Santiago, Chile. The equipment used was a shake table MOOG® model 6DOF2000E (Figure 11c) with a maximum capacity of 10 kN. This shaking table can reproduce peak accelerations up to 0.6g and displacements up to 0.25 meters.

The six R4SD were anchored and oriented in the principal axes of the shake table (Figure 11c). In addition, three orthogonally Episensor ES-U2 accelerometers were attached in the same directions. This way, it was possible to compare the seismic records related to the three MEMS accelerometers of each R4SD with those measured by the high-quality Episensor accelerometers. A sequence of three seismic records was simulated twice on the shake table scaled to 70% amplitude (seismic records related to Constitution Station for the Maule, Chilean earthquake Mw=8.8 in 2010, Concepcion Station for the Maule, Chilean earthquake Mw=8.8 in 2010, and Kobe Station for Hanshin-Awaji, Japanese earthquake Mw=6.9 in 1995). Figure 11a shows the time acceleration traces recorded by one Episensor ES-U2 and the MEMS R4SD accelerometer related to the North-South direction during the shake table tests associated with the seismic event of Constitution Station for the Maule, Chile earthquake Mw=8.8 in 2010. Note that the acceleration traces related to the Episensor accelerometer was filtered with a Butterworth low-pass filter with a cutoff frequency of 40Hz (N=8). Figure 11b shows the transfer function, coherence, and power spectral density related to the comparison.

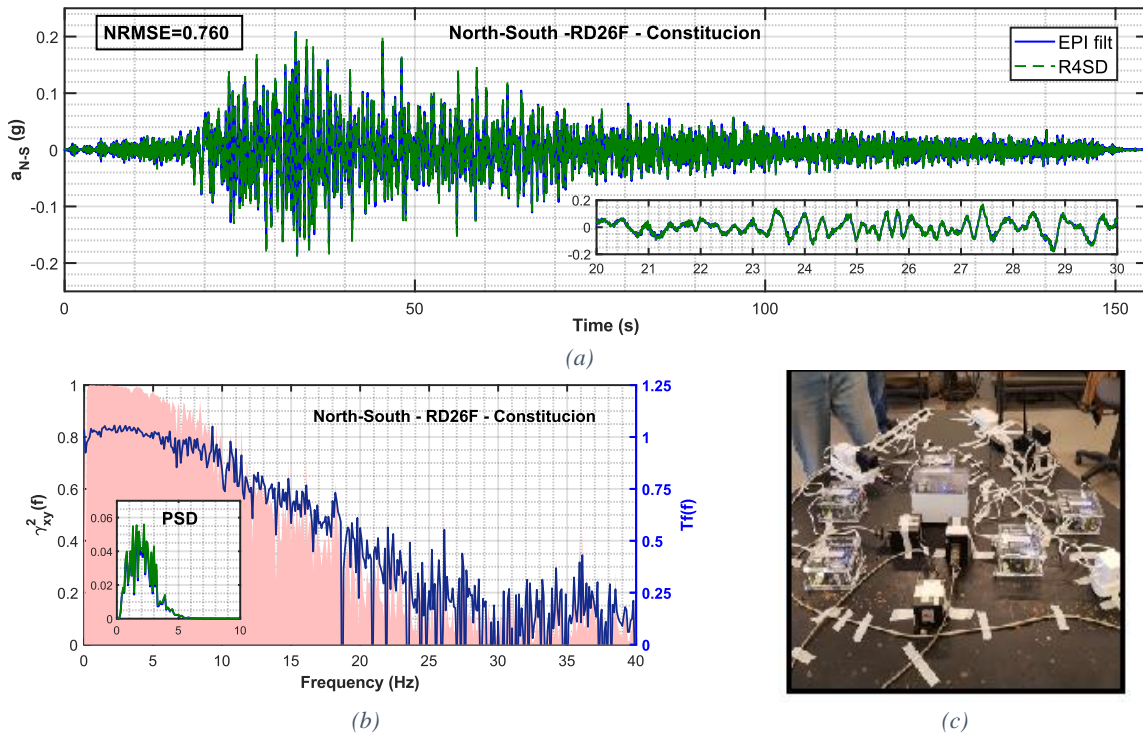


Figure 11: (a) Record comparison Episensor® ES-U2 vs. R4SD V8 accelerometers (signals filtered with a low-pass Butterworth $N=12$ at 25 Hz); (b) Transfer function, coherence, and PSD; (c) Shake table test

An evident coherence between the records obtained by the R4SD and the Episensor ES-U2 accelerometers can be observed. Furthermore, the shake table was able to reproduce significant energy until a maximum frequency of 5-7 Hz. It is therefore concluded that the LCSIS can accurately reproduce signals up to a frequency of approximately 20-25Hz. In addition, it was noticed that, on average, the MEMS accelerometers recorded an acceleration 2% higher than the recorded by the Episensor accelerometers. It was found that the vertical geophones, which were incorporated in the R4SD, were saturated (i.e., their values cannot be higher than their thresholds equal to 21 mm/s) during the shake table tests, which confirms that they can only be used for small seismic events or ambient vibration measurements. Similar results were observed for all R4SD instruments, all channels (North-South, East-West, and Vertical), and all seismic events studied in the shake table. Moreover, the NTP server proved that the instruments were adequately synchronized.

On October 23, 2021, the instrumentation network recorded the first seismic event in the Peñuelas tower. It was a seismic event $M_w=4.6$ that occurred 22 kilometers northwest of the city of El Tabo, Chile. This event allowed for comparing the time-acceleration traces (Figure 12) recorded by the R4SD accelerograph and the QDR equipment (Figure 7f) related to a low-intensity seismic event. Figure 12 also shows the absolute acceleration response spectrum ($\zeta=5\%$), the transfer function, coherence, and Power Spectral Density comparison. Overall, both sensors showed similar time acceleration traces ($NRMSE=0.684$), with a peak acceleration of 0.045g for QDR and 0.053g for R4SD. Both sensors exhibited a similar frequency content observing that the signal was governed by high-frequency components ($\sim 7-10$ Hz). The coherence and transfer function became consistent when the PSD displayed relevant energy and turned incoherent for frequencies that were not contained in the recorded signal. However, it can be observed that lower amplitudes for the QDR equipment at higher frequencies can be attributed to the intrinsic filter generated by this accelerograph (it also could explain differences in the peak acceleration values). Therefore, it can be concluded that LCSIS can

record high and intermediate acceleration motions based on the comparison observed from the shake table tests and the recorded signals measured in the field.

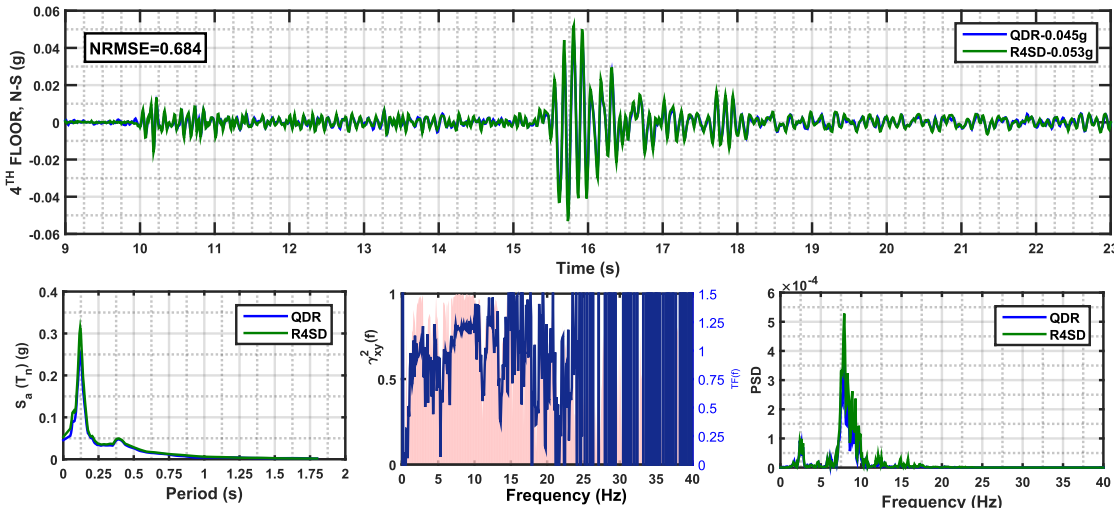


Figure 12: Seismic Record Comparison R4SD vs QDR, 4th Floor North-South, seismic event 2021/10/23 Mw=4.6

6 Structural Health Monitoring Implementation and Results

Based on the LCSIS described in Section 4, an SHM was implemented. The AV data was processed using the FDD method [41], which was programmed in the free software package Octave [53]. Figure 14b shows the semi-log plot related to the singular values of 29/04/2022 17:00 UTC time obtained from vertical R4SD geophones. Then, the first three natural frequencies of the Tower were estimated. Simultaneously, this routine called the BME280 sensor to evaluate the current temperature and relative humidity. As a result, a text file saved the history of estimated natural frequencies and environmental parameters on an hourly basis. The top plot of Figure 13 shows the temperature and relative humidity that the BME280 sensor recorded between 11/29/2021 and 07/06/2022 (i.e., environmental parameters recorded inside the building over floor 1). Similarly, the bottom plots in Figure 13 display the time-evolution of the natural frequencies related to the first three structural modes identified using the FDD method.

Significant variations of the natural frequencies were observed because of changes in the environmental conditions, see Figure 13. Similarly, Figure 14a displays the fluctuation of the natural frequencies and the recorded environmental parameters during the first week of 2022, showing that significant cyclic variations were observed daily. That is, the first natural frequency ranged between 1.95 and 2.50 Hz (28.2%) during the seven months analyzed, and a peak-to-peak daily variation of 10.9% was observed. The second natural frequency ranged between 2.66 and 3.33 Hz (25.2%), with a peak-to-peak daily variation of 9.5%. The third natural frequency fluctuated between 2.79 and 3.60 Hz (29.0%), showing a peak-to-peak daily variation of 10.3%. It was therefore observed that the shifts of the three natural frequencies followed a similar pattern.

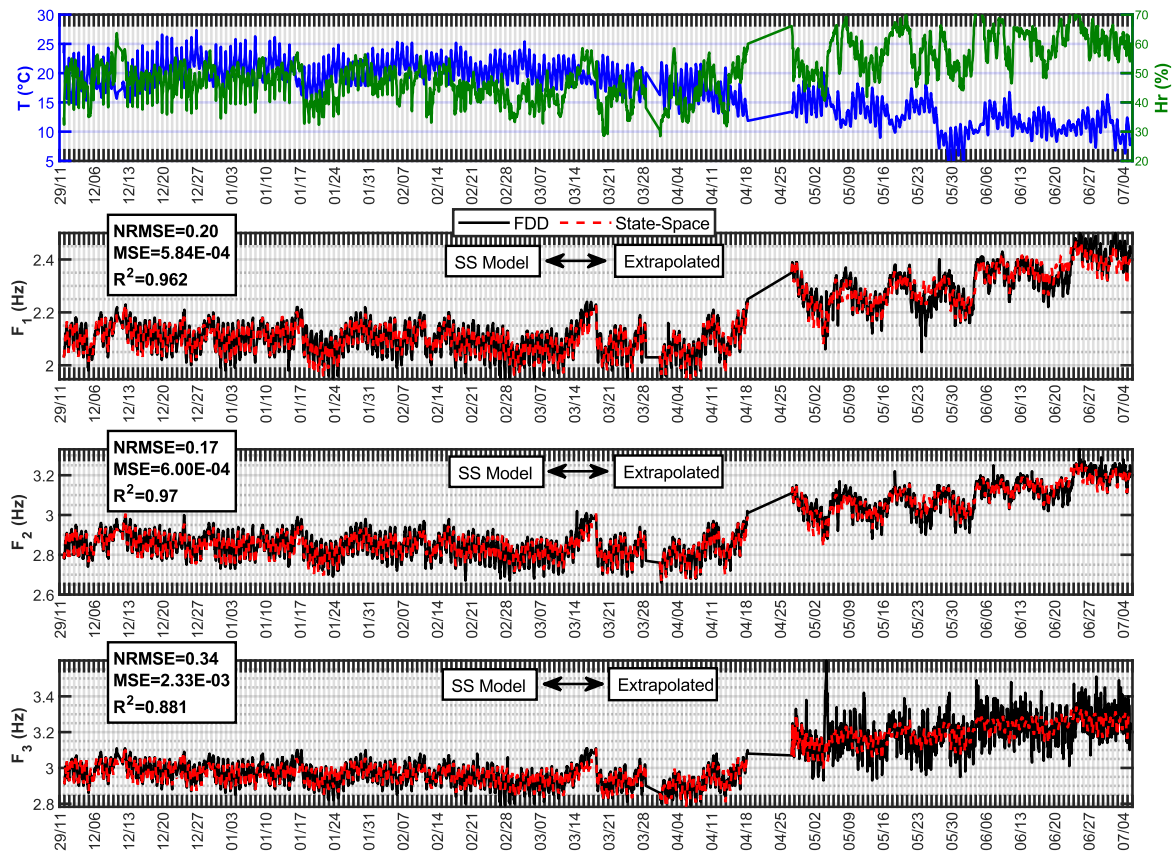


Figure 13: Internal temperature and relative humidity and first three principal natural frequencies identified from the FDD method [41] between 11/29/2021 to 07/06/2022 UTC Time

A poorly correlated relationship between the measured internal temperature and relative humidity was found, see Figure 14c, i.e., a lower relative humidity was monitored when higher internal temperatures were measured as a general trend. Figure 14c shows a third-degree polynomial with $R^2=0.49$ (the green lines correspond to the 95% confidence interval assuming a normal distribution). A few interruptions of the LCSIS measurement due to installation errors occurred because one of the accelerographs worked intermittently, see Figure 13. However, these errors in the novel system were fixed by changing the system identification routines to work even if one or multiple accelerographs were not working correctly, and the electrical connection of the corrupt accelerographs was fixed.

Regarding the relationship between the first three natural frequencies and ambient conditions, see Figure 15, it was found that the natural frequencies tend to be smaller at higher temperatures, and they tend to be higher for greater relative humidity. While the temperature result is as expected, since timber becomes less stiff at higher temperatures [54], this result is counterintuitive regarding the humidity, as timber also becomes less stiff with higher moisture [54]. In this regard, it needs to be pointed out that, on the one hand, there is an expected delay between ambient moisture and timber moisture, as the sorption and desorption process of wood typically takes a certain period of time [54]. Mainly depending on the moisture and temperature gradients, ambient pressure, and porosity of the wood [54]. However, a possible reason for this unexpected result may be that even when timber becomes less stiff when moist, it also swells, which may have a significant influence on the tightening, and thus, leading to a stiffening of the timber structural assemblies. These phenomena could be happening especially in bolted connections or other mechanical connections where clearance tolerances in the fasteners may be significantly affected depending on the timber moisture. Indeed, according to the Chilean standard NCh1198, the Chilean radiata pine would change its internal

moisture by approximately 4% if reaching equilibrium moisture when changing an extreme ambient relative humidity from 40% to 62.5% (see the recorded ambient relative humidity variance in Figure 14c). Such 4% of timber moisture variation would cause swelling and shrinking of about 1% in the timber member's cross-section according to the Chilean standard NCh1198. Such fluctuation in the cross sections may significantly affect the stiffness of specific assemblies, such as the wall-to-slab-to-wall assemblies and the clearance of bolted connections. Whatever the reason for this moist stiffening is, Figure 15 evidence that there is an influence of both the temperature and relative humidity on the natural frequency. Actually, the correlation for estimating the first natural frequency was similar for the relative humidity, $R^2=0.74$ compared to the correlation with temperature, i.e., 0.75. Therefore, it is observed that both parameters offer a similar accurateness to estimate the natural frequencies of timber structures if significant fluctuations of environmental conditions take place.

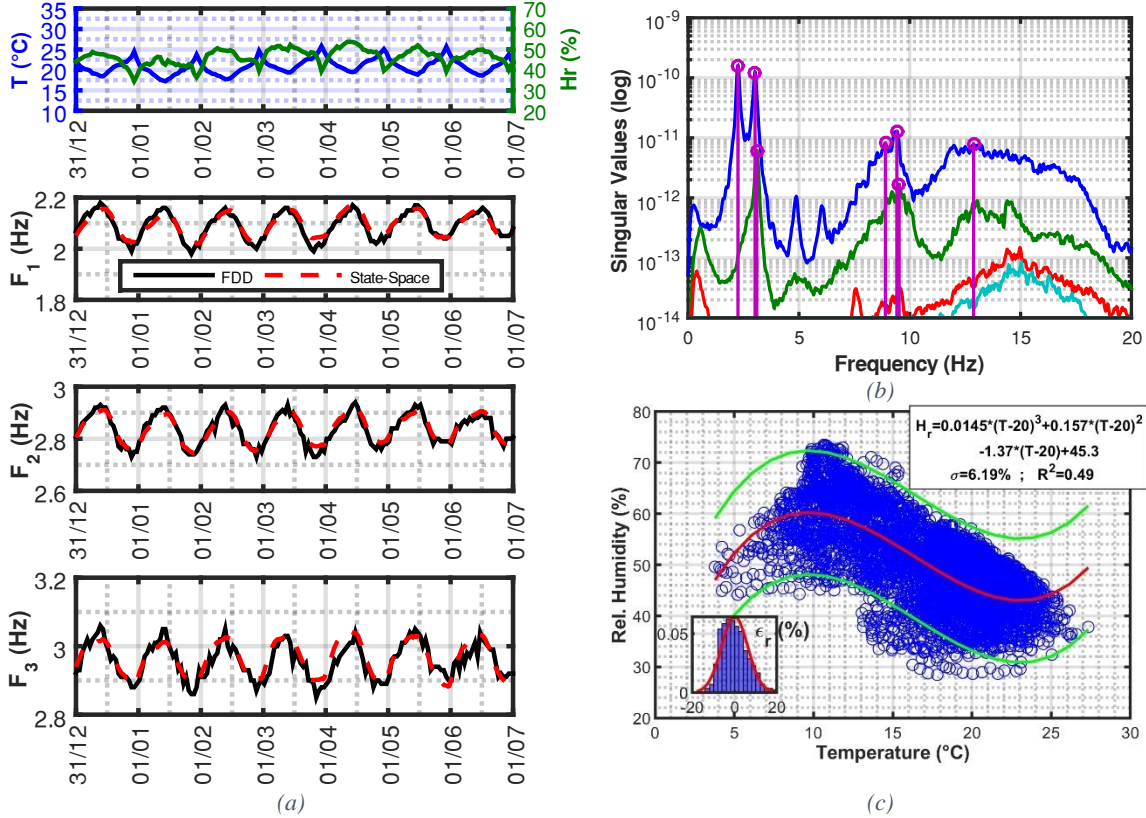


Figure 14: (a) Internal temperature, relative humidity, and natural frequencies identified from the FDD method during the first week of 2022. (b) Singular Values from the FDD method obtained from R4SD geophones, (c) Overall relationship between rel. Humidity and temperature were recorded inside the Peñuelas Tower

Based on the fact that natural frequencies depend on both environmental parameters (internal temperature and relative humidity) and observing that these natural frequencies seem to rely on the history of these parameters, a dynamic discrete-time subspace State-Space model (n4sid function from MATLAB) was adjusted to estimate each natural frequency as a function of the last 24-hour data related to the internal temperature and relative humidity, as follows,

$$\begin{aligned} x_{k+1} &= \mathbf{A} \cdot x_k + \mathbf{B} \cdot u_k + \mathbf{K} \cdot \varepsilon_k \\ F_k &= \mathbf{C} \cdot x_k + \mathbf{D} \cdot u_k + \varepsilon_k + \bar{F}_k \end{aligned} \quad (1)$$

Where x_k is the space-state vector (24x1) at the current time, ε_k = the current estimation error (1x1) - which is consequently minimized-, $\mathbf{A}, \mathbf{B}, \mathbf{C}, \mathbf{D}$ and \mathbf{K} are the state-space matrices that are adjusted and describe the dynamic system (24x24, 24x2, 1x24, 1x2, 24x1 respectively) -they were estimated

individually for each natural frequency-, $u_k = \{T_k, Hr_k\}^T$ is the input-variable parameters related to the current internal temperature and relative humidity, F_k is the measured or estimated natural frequency, and \bar{F}_k is the average natural frequency value (that is subtracted to data before to perform the SS model estimation, and consequently added to the SS model estimation).

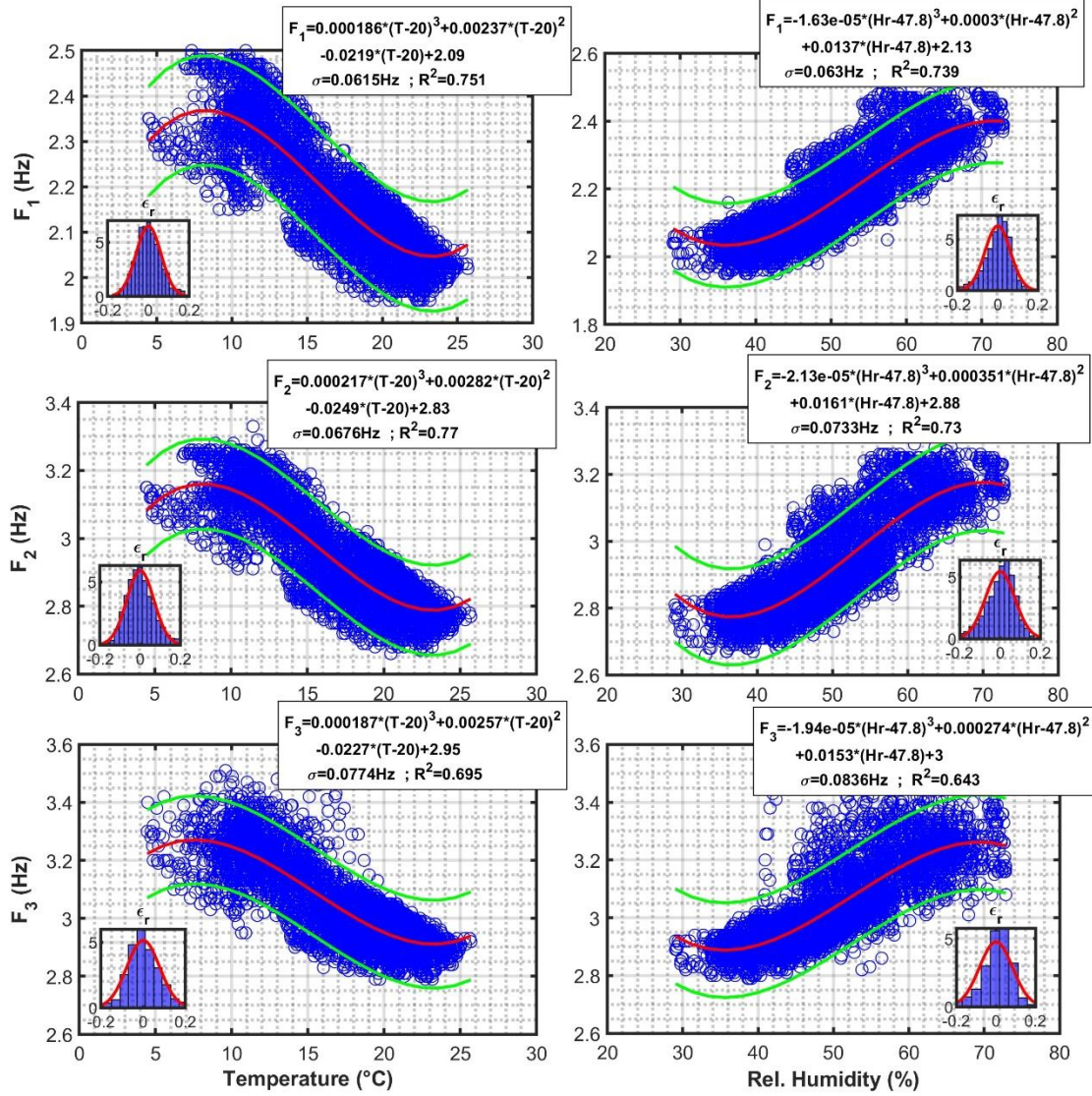


Figure 15: Polynomial estimation of natural frequencies from independent temperature and relative humidity parameters

Figure 13 and Figure 14a display in red lines the natural frequencies estimated by the state-space (SS) models constructed from data between 11/29/2021 and 03/14/2022, i.e., the SS model was built using approximately half of the current data. Based on this SS model, the natural frequencies related to the available data were evaluated in these plots for comparison, i.e., natural frequencies between 03/15/2022 to 07/06/2022 were extrapolated and compared with the SS model estimation. This comparison evidences that the system can correctly extrapolate data even for parameters out of the range of the data employed to build the model, i.e., the SS model estimated from data collected for summertime was accurately used for estimating the winter results. Similarly, the SS model estimates the initial condition for each data set (these sets of data were generated because of involuntary system interruptions). A comparison of the natural frequencies obtained with the FDD method and the natural frequencies adjusted with the SS model for the complete data is presented in Figure 16. It can

be observed that this model produces an accurate model with slight dispersion. Figure 13 and Figure 16 show that the normalized root mean square error (NRMSE) ranges between 0.20 to 0.34, the mean square error (MSE) fluctuates between $7.81E-4$ and $2.33E-3$, and the coefficient of determination ranges from 0.88 to 0.96 for the full set of data. Therefore, the adjusted SS models allow a reliable estimation of the natural frequencies as a function of the last 24 hours' internal temperature and relative humidity values. Figure 16 also shows the error distribution of the estimated frequencies ($\epsilon_i = F_i^{(est)} - F_i \forall i=1,2,3$), whose dispersion was significantly smaller than the polynomial fitted curves (Figure 15). The SS model still displays errors that may be explained because other environmental parameters are not accounted for (e.g., external temperature, external relative humidity, timber moisture, soil humidity, parameters related to other stories, wind speed, etc.), as well as it may be intrinsic numerical errors related to the used system identification technique.

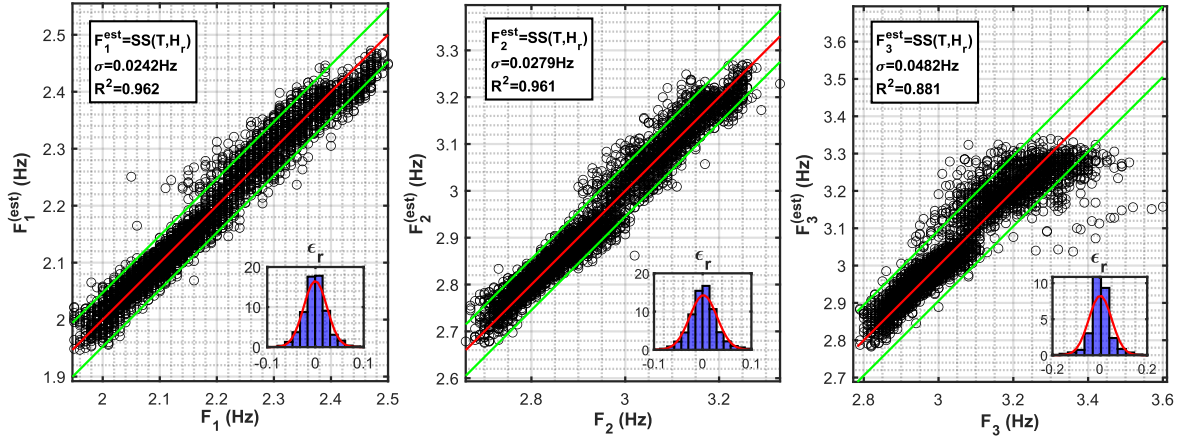


Figure 16: State-Space Estimated natural frequencies v/s FDD natural frequencies and natural frequency error distribution

The natural frequencies estimated from the FDD method as a function of the instantaneous internal temperature and relative humidity with scatter points are shown in Figure 17. As a comparison, Figure 17 shows the pseudo-static natural frequencies (F_k^{static}) estimation inferred from the SS models assuming that the environmental parameters remain constant for 24 hours (static assumption). That is, the pseudo-static natural frequencies can be estimated from the State-Space matrices, which is described as a flat surface. Thus, it can be concluded that the natural frequencies depend on both environmental parameters. Moreover, the differences between the natural and pseudo-static frequencies estimated from the SS models indicate that the natural frequencies of the Peñuelas Tower also depend on a dynamic component, i.e., the history of the environmental parameters.

The presented SS models could be used to evaluate the initial natural frequencies that may be used for further seismic analyses. Moreover, any change that the structure may experience could be hypothetically detected if a difference between the natural frequencies estimated by the FDD method differs from the values suggested by the SS model. For example, it is expected to observe a difference in the natural frequency values after an important seismic event (e.g., the mean value of the error presented in Figure 16 becomes different than zero with a new set of data after an earthquake); therefore, a non-zero mean error should be related to the actual changes in natural frequencies (residual stiffness degradation) that can be generated by structural damage. Hence, the SS model should serve to disaggregate the variation of natural frequencies that the Tower may naturally experience due to changes in its environmental conditions, stiffness degradation, or damage. Furthermore, the SS model can be periodically used to evaluate possible changes in the structure's natural frequencies. Thus, it shall enable checking any variation of its state to generate a structural health monitoring system that becomes independent of the environmental condition parameters.

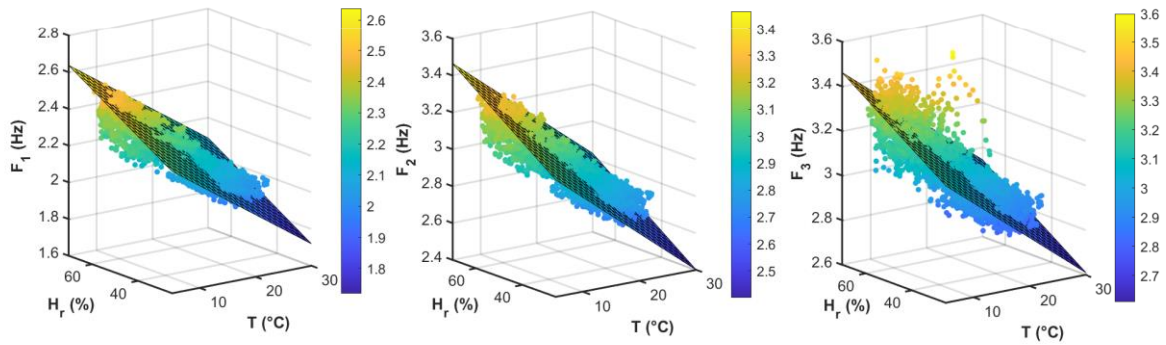


Figure 17: Natural frequency v/s instant temperature and relative humidity (scatter points) and State-Space model estimation assuming permanent environmental parameters (static assumption)

7 Conclusions

Low-cost seismic instrumentation (LCSIS) of the Peñuelas Tower was implemented using R4SD accelerographs, offering an affordable alternative to carrying out the instrumentation of structures in countries prone to high seismic activity. In addition, several aspects of the seismic instrumentation were described to provide effective remote control, communication, automatic data processing, synchronization, electric autonomy, seismic alert, and adding complementary sensors (e.g., the environmental sensor BME280) to the seismic instrumentation.

The seismic data recorded by the MEMS accelerometers incorporated in the R4SD-V8 instruments showed high accuracy based on the comparison of acceleration traces recorded in a shake table for strong motions (with Episensors ES-U2 accelerometers) and from data of a small seismic event ($M_w=4.6$) recorded in the Peñuelas Tower (with QDR accelerographs). Overall, the seismic data showed a high sensitivity for seismic signals up to 25-30 Hz.

Although the geophones incorporated in the R4SD instrument are vertically oriented, they were effectively employed to track the variation of the Peñuelas Tower dynamic properties from hourly ambient vibration tests. In fact, a campaign of five ambient vibration tests was performed in the Peñuelas Tower using highly sensitive Episensor US-E2 accelerometers, which allowed estimating the natural frequencies of the Tower and generating a full 6DOF representation of its mode shapes. It was observed that the mode shapes displayed significant vertical participation due to the high slenderness of the building; therefore, the vertical geophones could be effectively used to track the evolution of the dynamic properties of the Tower during the time. Moreover, the ambient vibration campaign showed that the natural frequencies varied substantially between different testing days (3-7%). In this context, the permanent instrumentation showed that changes in the environmental conditions could generate the frequency fluctuations observed during the different testing days. That is, the natural frequencies observed during the ambient vibration campaign were in the range of variation displayed when the SHM system was later implemented with the permanent seismic instrumentation.

The three principal natural frequencies of the Peñuelas Tower were identified using the FDD method from ambient vibration data collected and processed by the system on an hourly basis. In addition, the Peñuelas Tower's internal temperature and relative humidity were simultaneously monitored using an additional BME280 sensor (installed in an auxiliary RPi3). It was evidenced that the natural frequencies could vary significantly because of environmental changes. The natural frequencies become higher under moist and cold ambient. Peak-to-peak daily variation of the natural frequencies was as significant as 9.5-10.9%. Similarly, a variation of 25.2-29% of the extreme values of natural frequencies was observed during the seven months of monitoring. Therefore, it can be concluded that

the dynamic properties of timber structures could be more susceptible to environmental conditions than other structural systems, considering that this result can be expected based on wood's organic and hygroscopic nature. While it was expected to measure stiffer timber structures under cold conditions, it was unexpected to find higher frequencies under moist ambient. A reason for this counterintuitive finding may be attributed to the tightening and thus stiffening of timber assemblies due to the cross-sectional timber swelling when moist, especially at wall-to-slab-to-wall assemblies, as well as mechanical connections with clearance holes such as bolted connections.

State-Space models (SS) were effectively built to compute the natural frequencies of the Peñuelas Tower as a function of the last 24 hours' internal temperature and relative humidity data. This mechanism verified that the natural frequencies depend on both environmental parameters, and they also depend on the history of these values (dynamic effect). Finally, it was found that the State-Space models can be used to disaggregate the effect of the environmental conditions, allowing the implementation of a Structural Health Monitoring system to track dynamic property variations due to other sources (e.g., damage due to seismic loads).

Given the results of this investigation, it is expected to increase LCSIS in coupling with ambient measurements and SS models to enhance the structural health monitoring of timber structures. Furthermore, future investigations should investigate the application of the presented methods for quantifying structural damage in timber assemblies, as well as a better understanding of the effect of ambient conditions, especially regarding the stiffening of moist timber structures.

8 Acknowledgments

The authors acknowledge the support of the National Excellence Center for the Wood Industry (CENAMAD, ANID-BASAL FBA210015) and the Timber Innovation Center UC (CIM UC).

9 Bibliography

- [1] H. Svatoš-Ražnjević, L. Orozco, A. Menges, Advanced Timber Construction Industry: A Review of 350 Multi-Storey Timber Projects from 2000–2021, *Buildings*. 12 (2022) 404. <https://doi.org/10.3390/buildings12040404>.
- [2] V.Ž. Leskovar, M. Premrov, A review of architectural and structural design typologies of multi-storey timber buildings in Europe, *Forests*. 12 (2021). <https://doi.org/10.3390/f12060757>.
- [3] N.C. Onat, M. Kucukvar, Carbon footprint of construction industry: A global review and supply chain analysis, *Renew. Sustain. Energy Rev.* 124 (2020) 109783. <https://doi.org/10.1016/j.rser.2020.109783>.
- [4] A.H. Buchanan, S.B. Levine, Wood-based building materials and atmospheric carbon emissions, *Environ. Sci. Policy*. 2 (1999) 427–437. [https://doi.org/10.1016/S1462-9011\(99\)00038-6](https://doi.org/10.1016/S1462-9011(99)00038-6).
- [5] T. Yipintsoi, *Wood Handbook: Wood as an Engineering Material*, 2010. <https://doi.org/10.1161/01.RES.39.4.523>.
- [6] A. Wenzel, S. Vera, P. Guindos, Integration of energy and seismic-structural design variables through the optimization of a multi-story residential light-frame timber building with different seismic lateral connectors and building stories, *J. Build. Eng.* (2022).
- [7] AWC-American Wood Council, *National Design Specification*, 2018.
- [8] Eurocode 5: Design of timber structures - Part 1-1: General - Common rules and rules for buildings, 2004.
- [9] B.R. Ellis, A.J. Bougard, Dynamic testing and stiffness evaluation of a six-storey timber framed building during construction, *Eng. Struct.* 23 (2001) 1232–1242. [https://doi.org/10.1016/S0141-0296\(01\)00033-5](https://doi.org/10.1016/S0141-0296(01)00033-5).
- [10] V. Camelo, *Dynamic Characteristics of Woodframe Buildings*, California Institute of Technology, 2003. papers3://publication/uuid/42491117-3BF3-4383-866B-4093C1FFB83.
- [11] G. Hafeez, G. Doudak, Establishing the fundamental period of light-frame wood buildings on the basis of ambient vibration tests, *Can. J. Civ. Eng.* 45 (2018) 752–765. <https://doi.org/10.1139/cjce-2017-0348>.
- [12] G. Hafeez, G. Doudak, G. McClure, *Dynamic Characteristics of Light-Frame Wood Buildings*, *Can. J. Civ. Eng.* (2018).
- [13] H. Sun, O. Büyüköztürk, The MIT Green Building benchmark problem for structural health monitoring of tall buildings, *Struct. Control Heal. Monit.* 25 (2018) 1–17. <https://doi.org/10.1002/stc.2115>.
- [14] M.P. Limongelli, M. Çelebi, *Seismic Structural Health Monitoring: From Theory to Successful Applications*, 2019. <https://doi.org/10.1007/978-3-030-13976-6>.
- [15] C. Wang, J. Xiao, C. Zhang, X. Xiao, Structural health monitoring and performance analysis of a 12-story recycled aggregate concrete structure, *Eng. Struct.* 205 (2020) 110102. <https://doi.org/10.1016/j.engstruct.2019.110102>.
- [16] W.M. González, R.L. Boroschek, J.A. Bilbao, Temperature measurement assisted modal

- tracking of an instrumented building, *Eng. Struct.* 233 (2021). <https://doi.org/10.1016/j.engstruct.2021.111907>.
- [17] L.F. Ramos, R. Aguilar, P.B. Lourenço, S. Moreira, Dynamic structural health monitoring of Saint Torcato church, *Mech. Syst. Signal Process.* 35 (2013) 1–15. <https://doi.org/10.1016/j.ymsp.2012.09.007>.
- [18] A. De Stefano, E. Matta, P. Clemente, Structural health monitoring of historical heritage in Italy: some relevant experiences, *J. Civ. Struct. Heal. Monit.* 6 (2016) 83–106. <https://doi.org/10.1007/s13349-016-0154-y>.
- [19] J.M. Ko, Y.Q. Ni, Technology developments in structural health monitoring of large-scale bridges, *Eng. Struct.* 27 (2005) 1715–1725. <https://doi.org/10.1016/j.engstruct.2005.02.021>.
- [20] S. Beskhyroun, L.D. Wegner, B.F. Sparling, Structural health monitoring of the Tamar suspension bridge, *Struct. Control Heal. Monit.* (2011) n/a-n/a. <https://doi.org/DOI:10.1002/stc.1481>.
- [21] H.-P. Chen, *Structural Health Monitoring of Large Civil Engineering Structures*, 2018.
- [22] M.H.K. Kharrazi, *Vibration Characteristics of Single-Family Woodframe Buildings*, The University of British Columbia, 2001.
- [23] A. Filiatrault, D. Fischer, B. Folz, C.-M. Uang, Seismic Testing of Two-Story Woodframe House: Influence of Wall Finish Materials, *J. Struct. Eng.* 128 (2002) 1337–1345. [https://doi.org/10.1061/\(asce\)0733-9445\(2002\)128:10\(1337\)](https://doi.org/10.1061/(asce)0733-9445(2002)128:10(1337)).
- [24] I.P. Christovasilis, A. Filiatrault, A. Wanitkorkul, Seismic Testing Of A Full-Scale Wood Structure On Two Shake Tables, 14th World Conf. Earthq. Eng. (2008). http://www.iitk.ac.in/nicee/wcee/article/14_S12-001.PDF.
- [25] J.W. van de Lindt, S. Pei, S.E. Pryor, H. Shimizu, H. Isoda, Experimental seismic response of a full-scale six-story light-frame wood building, *J. Struct. Eng.* 136 (2010) 1262–1272. [https://doi.org/10.1061/\(ASCE\)ST.1943-541X.0000222](https://doi.org/10.1061/(ASCE)ST.1943-541X.0000222).
- [26] U.S. Geological Survey, *Advanced National Seismic System—Current status, development opportunities, and priorities for 2017–2027*, 2017.
- [27] A. Manconi, V. Coviello, M. Galletti, R. Seifert, Short communication: Monitoring rockfalls with the Raspberry Shake, *Earth Surf. Dyn.* 6 (2018) 1219–1227. <https://doi.org/10.5194/esurf-6-1219-2018>.
- [28] R.E. Anthony, A.T. Ringler, D.C. Wilson, E. Wolin, Do low-cost seismographs perform well enough for your network? An overview of laboratory tests and field observations of the OSOP raspberry shake 4D, *Seismol. Res. Lett.* 90 (2019) 219–228. <https://doi.org/10.1785/0220180251>.
- [29] J.J. Ugarte, E. Wiegand, J. Montaña, S. Cárcamo, C. Delucchi, Light frame timber tower: Interdisciplinary design of prefabricated and anti-seismic 5-story experimental building, *WCTE 2018 - World Conf. Timber Eng.* (2018).
- [30] Australian/New Zealand: *Timber-Stress-graded-Ing-grade strength and stiffness evaluation*, 1992.
- [31] EN 14081-1:2016 *Timber structures - Stregnth graded structural timber with rectangular cross section - Part 1: General requirements*, 2016.
- [32] A. The Engineered Wood Association, *PS2-18 Performance Standard for Wood Structural*

Panels, 2018.

- [33] A. The Engineered Wood Association, PS1-19 Structural Plywood, 2019. www.CORRIM.org.
- [34] X. Estrella, S. Malek, J.L. Almazán, P. Guindos, H. Santa María, Experimental study of the effects of continuous rod hold-down anchorages on the cyclic response of wood frame shear walls, *Eng. Struct.* 230 (2021). <https://doi.org/10.1016/j.engstruct.2020.111641>.
- [35] X. Estrella, P. Guindos, J.L. Almazán, S. Malek, Efficient nonlinear modeling of strong wood frame shear walls for mid-rise buildings, *Eng. Struct.* 215 (2020). <https://doi.org/10.1016/j.engstruct.2020.110670>.
- [36] A. Sadeghi Marzaleh, S. Nerbano, A. Sebastiani Croce, R. Steiger, OSB sheathed light-frame timber shear walls with strong anchorage subjected to vertical load, bending moment, and monotonic lateral load, *Eng. Struct.* 173 (2018) 787–799. <https://doi.org/10.1016/j.engstruct.2018.05.044>.
- [37] F. Guñez, H. Santa María, J.L. Almazán, Monotonic and cyclic behaviour of wood frame shear walls for mid-height timber buildings, *Eng. Struct.* 189 (2019) 100–110. <https://doi.org/10.1016/j.engstruct.2019.03.043>.
- [38] J.J. Ugarte, J. Montañó, E. Wiegand, E. Serra, S. Carcamo, C. Delucchi, J. Lagos, WOOD LIGHT-FRAME MID-RISE BUILDING ASSEMBLY AND ERECTION PRODUCTIVITY, WCTE 2020 - World Conf. Timber Eng. (2020).
- [39] U. Force, B. Accelerometer, ES-U2 Uniaxial Force Balance Accelerometer, (n.d.).
- [40] P. Van Overschee, B. De Moor, Subspace Identification for Linear System: Theory - Implementation - Applications, Kluwer Academic Publishers, 1996.
- [41] P. Brincker, Rune; Ventura, C. E.; Andersen, Damping Estimation by Frequency Domain Decomposition, in: IMAC 19 A Conf. Struct. Dyn., Kissimmee, Florida, 2001: pp. 698–703.
- [42] R.J. Allemang, D.L. Brown, A correlation coefficient for modal vector analysis, *First Int. Modal Anal. Conf.* (1982) 110–116.
- [43] C.S.A. (CSA), Engineering Design in wood, Ontario, Canada, 2014.
- [44] Raspberry Shake, Raspberry Shake Main Page, (2022). <https://raspberrysshake.org>.
- [45] Raspberry Shake, Specifications for : Raspberry Shake RS4D, (2021).
- [46] AnyDesk, AnyDesk: Remote desktop software, (n.d.). <https://anydesk.com>.
- [47] S. Tatham, PuTTY User Manual, (2017). <https://www.putty.org>.
- [48] Filezilla, Filezilla-Project: Open source FTP and FTPS Server, (n.d.). <https://filezilla-project.org>.
- [49] The ObsPy Development Team, ObsPy tutorial release 1.2.0, (2020). <https://docs.obspy.org>.
- [50] Alaska Volcano Observatory, Seismic wave analysis and real-time monitor: user manual and reference guide, version 3.1.0, (2020).
- [51] F.L. Van Rossum, Guido and Drake Jr, Python reference manual, Cent. Voor Wiskd. En Inform. Amsterdam. (1995). <https://www.python.org>.
- [52] Kinometrics, Kinometrics QDR Quake Data Recorder Document 3025704 Revision E, (2001) 1–124.

- [53] J.W. Eaton, GNU Octave Manual, (2002). <https://www.gnu.org/software/octave/index>.
- [54] P. Guindos, Fundamentos del diseño y la construcción con madera, First edit, Ediciones UC, 2019.